

# Synthesis of the first nitrogen-heterocycles in interstellar ice analogs containing methylamine ( $\text{CH}_3\text{NH}_2$ ) exposed to UV radiation: Formation of trimethylentriamine (TMT, $\text{c-}(-\text{CH}_2-\text{NH})_3$ ) and hexamethylenetetramine (HMT, $(\text{CH}_2)_6\text{N}_4$ ).

H. Carrascosa,<sup>1</sup>★ C. González Díaz,<sup>1</sup> G. M. Muñoz Caro,<sup>1</sup>† P. C. Gómez,<sup>2</sup> M. L. Sanz,<sup>3</sup>

<sup>1</sup>Centro de Astrobiología (CSIC-INTA), Ctra. de Ajalvir, km 4, Torrejón de Ardoz, 28850 Madrid, Spain

<sup>2</sup>Dep. Química Física, Fac. Química, Univ. Complutense, 28040 Madrid, Spain

<sup>3</sup>Department of instrumental analysis and environmental chemistry, IQOG-CSIC, Juan de la Cierva 3, 28006 Madrid, Spain

Accepted XXX. Received YYY; in original form ZZZ

## ABSTRACT

Hexamethylenetetramine has drawn a lot of attention due to its potential to produce prebiotic species. This work aims to gain a better understanding in the chemical processes concerning methylamine under astrophysically relevant conditions. In particular, this work deeps into the formation of N-heterocycles in interstellar ice analogs exposed to UV radiation, which may lead to the formation of prebiotic species.

Experimental simulations of interstellar ice analogs were carried out in ISAC. ISAC is an ultra-high vacuum chamber equipped with a cryostat, where gas and vapour species are frozen forming ice samples. Infrared and ultraviolet spectroscopy were used to monitor the solid phase, and quadrupole mass spectrometry served to measure the composition of the gas phase. The variety of species detected after UV irradiation of ices containing methylamine revealed the presence of 12 species which have been already detected in the ISM, being 4 of them typically classified as complex organic molecules: formamide ( $\text{HCONH}_2$ ), methyl cyanide ( $\text{CH}_3\text{CN}$ ),  $\text{CH}_3\text{NH}$  and  $\text{CH}_3\text{CHNH}$ . Warming up of the irradiated  $\text{CH}_3\text{NH}_2$ -bearing ice samples lead to the formation of trimethylentriamine (TMT), a N-heterocycle precursor of HMT, and the subsequent synthesis of HMT at temperatures above 230 K.

**Key words:** Astrochemistry – Methods: laboratory: molecular – techniques: spectroscopy – software: simulation – ultraviolet: ISM – ISM: molecules

## 1 INTRODUCTION

Molecules with six or more atoms including at least one C atom are known as complex organic molecules (COMs) (Herbst & van Dishoeck 2009). COMs have been detected in dense interstellar clouds and circumstellar regions. Deep inside dense clouds, the interstellar UV field cannot penetrate and dust temperature decreases to around 10 K. At these low temperatures,  $\text{H}_2\text{O}$  and other molecules including CO,  $\text{CO}_2$ ,  $\text{CH}_3\text{OH}$ ,  $\text{CH}_4$ , or  $\text{NH}_3$  accrete onto dust grains forming ice mantles. These ice mantles are exposed to secondary-UV photons generated by the interaction between cosmic rays and hydrogen molecules, as well as direct cosmic ray impact, producing radicals and ions which can lead to the formation of new species. Some intermediate species can react at low temperature, while others remain in the ice until the

temperature increases and thermal energy is enough to overcome the activation barriers to form new species. Up to now, more than 200 different molecules have been detected in the gas phase toward interstellar and circumstellar environments, including around 50 COMs. An important fraction of these species is thought to be produced in ice mantles.

Among them, methylamine ( $\text{CH}_3\text{NH}_2$ ) has drawn considerable attention due to its potential to produce prebiotic species. It was first detected in Sagittarius B2 and Orion A molecular clouds with column densities ranging from  $1 \times 10^{15} \text{ cm}^{-2}$  to  $4 \times 10^{15} \text{ cm}^{-2}$  (Kaifu et al. 1974; Fourikis et al. 1974; Bellocche et al. 2013). Goesmann et al. (2015) and Altwegg et al. (2017) reported  $\text{CH}_3\text{NH}_2$  abundances from 0.6% to 1.2% relative to  $\text{H}_2\text{O}$  on comet 67P/Churyumov-Gerasimenko. Finally,  $\text{CH}_3\text{NH}_2$  has been also detected in hot cores. Ohishi et al. (2019) reported the presence of  $\text{CH}_3\text{NH}_2$  in G10.47+0.03 while Bøgelund et al. (2019) observed column densities between  $3.0 \times 10^{15}$  and  $2.7 \times 10^{17}$  in three dif-

★ E-mail: hcarrascosa@cab.inta-csic.es

† E-mail: munozcg@cab.inta-csic.es

ferent hot cores from the high-mass star forming region NGC 6334I.

Different mechanisms have been proposed for methylamine formation under astrophysical conditions. In the gas phase, [Herbst \(1985\)](#) modelled the possible association between  $\text{CH}_3^+$  ions and  $\text{NH}_3$  molecules to produce  $\text{CH}_3\text{NH}_2$ , concluding that it was an efficient route to produce methylamine under interstellar conditions, despite the existence of exothermic reaction channels. [Gardner & McNesby \(1980\)](#) and [Ogura et al. \(1989\)](#) reported the formation of methylamine from photolysis of gas mixtures containing  $\text{CH}_4$  and  $\text{NH}_3$ . In their experiments, UV-irradiation produced  $\text{CH}_3\cdot$  and  $\text{NH}_2\cdot$  radicals able to recombine to produce  $\text{CH}_3\text{NH}_2$ . This pathway was also explored in ice samples by [Kim & Kaiser \(2011\)](#) and [Förstel et al. \(2017\)](#), who carried out electron bombardment and photon irradiation of  $\text{CH}_4:\text{NH}_3$  ice mixtures, respectively, reporting the formation of methylamine in both works. An alternative route is the successive hydrogenation of gas phase HCN molecules, analogous to the formation of  $\text{H}_2\text{CO}$  and  $\text{CH}_3\text{OH}$  from CO molecules, as pointed out by [Dickens et al. \(1997\)](#) and [Theule et al. \(2011\)](#).

Several experiments reveal the potential of  $\text{CH}_3\text{NH}_2$  to form prebiotic molecules. [Holtom et al. \(2005\)](#) prepared  $\text{CH}_3\text{NH}_2:\text{CO}_2$  binary ice mixtures which resulted in glycine ( $\text{NH}_2\text{CH}_2\text{COOH}$ ) formation under electron bombardment. [Bossa et al. \(2009a\)](#) reproduced the same ice mixture in a water dominated ice. They found evidence on the formation of methylammonium methylcarbamate,  $[\text{CH}_3\text{NH}_3^+][\text{CH}_3\text{NHCOO}^-]$ , a glycine salt precursor in astrophysical environments dominated by thermal and UV processing. In the same year, [Lee et al. \(2009\)](#) reported the formation of several COMs from UV irradiation of  $\text{CH}_3\text{NH}_2:\text{CO}_2$  mixtures on top of a  $\text{H}_2\text{O}$  ice.

The main motivation to study the UV-photoprocessing of methylamine-bearing ices in this work is to gain a better understanding on the formation of N-heterocycles in interstellar ice analogs. In particular, we targeted the synthesis of hexamethylenetetramine (HMT), a molecule commonly identified among the refractory products in ice irradiation experiments, and its precursor, trimethylentriamine (TMT).

Hexamethylenetetraamine ( $\text{C}_6\text{N}_4\text{H}_{12}$ , HMT) is a molecule of prime interest in astrochemistry. Firstly, it is a stable molecule efficiently made by UV or ion processing of interstellar ice analogs, which remains in the generated organic residue at room temperature ([Briggs et al. 1992](#); [Cottin et al. 2001](#)). Second, it may catalyze organic reactions leading to the formation of other COMs ([Vinogradoff et al. 2012](#)). Third, its acid hydrolysis leads to the formation of several aminoacids ([Fox & Windsor 1970](#)). HMT has been recently detected in Murchison ( $846\pm 37$  ppb), Murray ( $29\pm 9$  ppb) and Tagish Lake ( $671\pm 9$  ppb) carbonaceous chondrites, as well as the methyl, amino, hydroxy and hydroxymethyl derivatives of HMT (see [Oba et al. 2020](#)). The synthesis of HMT derivatives in ice irradiation experiments was previously reported ([Muñoz Caro et al. 2004](#); [Sandford et al. 2020](#); [Materese et al. 2020](#); [Urso et al. 2020](#)).

HMT can be produced from condensation reaction between ammonia and formaldehyde in aqueous solution ([Meissner et al. 1954](#), Fig. 1). This synthetic pathway has been typically applied to ice chemistry ([Bernstein et al. 1995](#); [Muñoz Caro & Schutte 2003](#); [Vinogradoff et al. 2013](#), and references therein). Basically, the proposed synthetic route is as follows.  $\text{CH}_3\text{OH}$  is easily dehydro-

genated by UV radiation to produce formaldehyde, or formaldehyde is formed, albeit less efficiently, from hydrogenation of CO in the ice ([Briggs et al. 1992](#); [Muñoz Caro & Schutte 2003](#); [Muñoz Caro et al. 2004](#)). The reaction between a carbonyl group and a primary amine typically leads to the formation of imine groups ( $\text{R}=\text{N}-\text{R}'$ ), releasing a water molecule. Thus, from formaldehyde and ammonia, methylenimine ( $\text{CH}_2\text{NH}$ ) is obtained. This highly reactive methylenimine polymerises, leading to a 6-member stable ring, known as trimethylenetriazine (TMT). Methylen groups are electron-deficient units which incorporate hydroxymethyl radicals to form 1,3,5-trihydroxymethyltrimethylenetriazine (TMT-triol). The latter leads to HMT in presence of ammonia. The last step, however, only takes place at high temperatures, when ammonia is already thermally desorbed to the gas phase in the ice irradiation and warm-up experiments. Indeed, [Muñoz Caro & Schutte \(2003\)](#) observed the formation of HMT at room temperature monitoring the growth of its main absorption bands in the IR spectra at 1007 and  $1234\text{ cm}^{-1}$ . These authors proposed the presence of carboxylate ammonium salts, which would remain in the ice at high temperature, able to provide the amino groups.

[Vinogradoff et al. \(2012, 2013\)](#) and references therein deepened in the formation mechanism of HMT. Those works reported measurements of complex ice mixtures, confirming that formaldehyde reacts with ammonia to produce methylenimine ( $\text{CH}_2\text{NH}$ ). However, the stability of organic rings favours the cyclation of the 6-member species  $\text{CH}_2\text{NH}-\text{CH}_2\text{NH}-\text{CH}_2\text{NH}$ , leading to the production of TMT ([Vinogradoff et al. 2012](#)). TMT is then converted into HMT near room temperature.

Within this work, we explore an alternative mechanism in the production of HMT. We have focused on the primary steps and the intermediate species. We have calculated the theoretical IR spectrum of TMT since we found no spectrum for this species in the literature. The validity of this calculation was checked comparing the calculated HMT spectrum to the one measured in the laboratory. [Gardner & McNesby \(1982\)](#) reported the preferential formation of  $\text{CH}_2\text{NH}$  from UV irradiation of  $\text{CH}_3\text{NH}_2$  molecules, supported by the efficient formation of  $\text{H}_2$  molecules. By using methylamine, we have been able to study in more depth the chemical pathways of C-N bearing molecules in different environments. Noble gas matrix isolation experiments were also carried out to isolate  $\text{CH}_2\text{NH}$  molecules, thus allowing the study of its spectroscopic features and radical formation. This will be explained in more detail in the paragraphs below.

In addition to the primary processes leading to HMT, we also studied the formation of other photoproducts arising upon UV irradiation of methylamine. When  $\text{H}_2\text{O}$  is added to  $\text{CH}_3\text{NH}_2$  in the ice, in a likely more realistic astrophysical scenario, oxygenated species are formed. Some of them, such as HCN, HNCO or  $\text{HCONH}_2$  were found in comet 67P/Churyumov-Gerasimenko surface during the Rosetta mission ([Goesmann et al. 2015](#)), and confirmed by [Altwegg et al. \(2017\)](#) using DFMS spectra from the orbiter. Finally, we produced a well-studied residue by irradiation of  $\text{H}_2\text{O}:\text{CH}_3\text{OH}:\text{NH}_3$  ice mixture for comparison with the methylamine ice experiments ([Bernstein et al. 1995](#); [Muñoz Caro & Schutte 2003](#); [Vinogradoff et al. 2013](#)).

The present paper is structured as follows. Sect. 2 explains the experimental procedure used during the experimental simulations, as well as the calculated IR spectra. Sect. 3 is divided into four

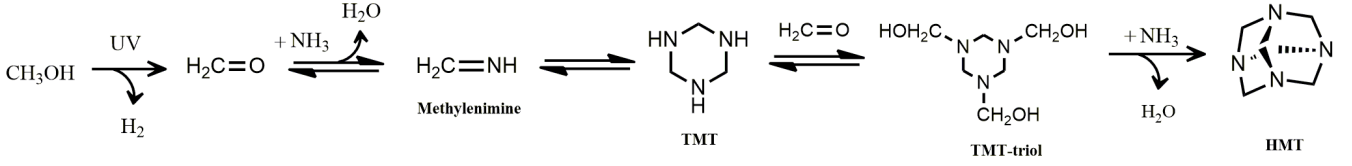


Figure 1. Synthetic pathway proposed for HMT synthesis.

subsections. Sect. 3.2 presents the different features of  $\text{CH}_3\text{NH}_2$  in the three environments studied in this work. Sect. 3.3 explores the different rate of  $\text{H}_2$  subtraction during UV irradiation of the different ice matrices. Sect. 3.4 focuses on the formation of photoproducts at 8 K in the different ice mixtures. Sect. 3.6 goes deeper into the formation of large species, such as TMT, which only takes place at higher temperatures. Finally, Sect. 4 and Sect. 5 summarizes the main results and present the astrophysical implications.

## 2 EXPERIMENTAL

### 2.1 ISAC experimental simulations

Experiments were carried out in the Interstellar Astrochemistry Chamber (ISAC), fully described in Muñoz Caro et al. (2010). ISAC is an Ultra-High Vacuum (UHV) chamber with a base pressure of  $4 \times 10^{-11}$  mbar equipped with a closed-cycle helium cryostat able to reach temperatures of 8 K in a  $\text{MgF}_2/\text{KBr}$  substrate used for ice deposition.

For the experiments, highly distilled MilliQ water was obtained from a Millipore water distribution system IQ-7000. For matrix experiments, Xe was acquired from Praxair with a 99.999% purity. Methylamine was purchased from Merck group diluted in water (40% in water solution). The higher vapour pressure of methylamine compared to the solvent allowed us to prepare relatively pure samples, as confirmed by infrared spectroscopy, although traces of water ( $\leq 5\%$ ) are assumed to be present in "pure" methylamine ices. Nevertheless, the low deposition rate in Xe isolated methylamine ice samples determined the absence of any water signals in the IR spectrum. For  $\text{H}_2\text{O}:\text{CH}_3\text{OH}:\text{NH}_3$  ice mixtures,  $\text{CH}_3\text{OH}$  was purchased from Panreac Quimica S.A. (99.9% purity) and  $\text{NH}_3$  from Air Liquide España S.A. ( $\geq 99.96\%$  purity).

Gases and vapours were introduced in the main chamber through a capillary tube of 1 mm internal diameter at normal incidence angle with respect to the  $\text{MgF}_2$  substrate at pressures ranging from  $2 \times 10^{-7}$  to  $1 \times 10^{-6}$  for the different experiments. To ensure the purity of the ice mixtures, a quadrupole mass spectrometer (QMS, Pfeiffer Vacuum, Prisma QMS 200) was placed in the injection system, thus avoiding any contamination and providing a method to achieve the desired ratio between the components. The gas phase was monitored continuously in the main chamber using another QMS (Pfeiffer Vacuum, Prisma QMS 200) equipped with a Channeltron detector. For matrix isolation experiments, Xe pressure (monitored by  $\frac{m}{z} = 131$ ) was adjusted to measure an ion current at least two orders of magnitude larger than the one measured for the most intense fragment from methylamine ( $\frac{m}{z} = 30$ ). In addition, Xe has three natural isotopes

with similar abundances, thus, the real ratio  $\text{Xe}:\text{CH}_3\text{NH}_2$  turned out to be around 10.000:1, providing a good isolation of  $\text{CH}_3\text{NH}_2$  molecules. This is supported by the disappearance of the N-H stretching vibrations in the IR spectrum, as explained in Sect. 3.2.

Fourier-transform infrared spectroscopy (FTIR) transmittance spectra were recorded using a Bruker VERTEX 70 with a resolution of  $1\text{--}2\text{ cm}^{-1}$ , equipped with a deuterated triglycine sulfate (DGTS) detector to monitor the solid phase. IR spectra of the ice samples were performed before and after deposition of the ice, after each irradiation interval, and during the warming up. From the infrared spectra, the column density was estimated following eq. 1, where  $A$  is the band strength in  $\text{cm molecule}^{-1}$ ,  $\tau_v$  is the optical depth, and  $d\nu$  is the wavenumber differential in  $\text{cm}^{-1}$ . For methylamine, the adopted band strength is the one reported by Holtom et al. (2005),  $4.3 \times 10^{-18}\text{ cm molecule}^{-1}$  for the  $1613\text{ cm}^{-1}$  IR band. For  $\text{H}_2\text{O}$ , a value of  $2.0 \times 10^{-16}\text{ cm molecule}^{-1}$  for its  $3259\text{ cm}^{-1}$  IR band was used (Hagen et al. 1981). For methanol,  $1.8 \times 10^{-17}\text{ cm molecule}^{-1}$  for its  $1025\text{ cm}^{-1}$  IR band (D'Hendecourt et al. 1986). Finally, for  $\text{NH}_3$ , a value of  $1.7 \times 10^{-17}\text{ cm molecule}^{-1}$  for its  $1070\text{ cm}^{-1}$  IR band was adopted (Sandford & Allamandola 1993).

$$N = \frac{1}{A} \int_{\text{band}} \tau_v d\nu. \quad (1)$$

For optically thick ices, the ratio between the components was estimated from the ion current measured by the QMS during the deposition of the ice samples, which showed a good agreement with the values calculated from IR spectroscopy.

Ice samples were irradiated with a F-type microwave discharged hydrogen lamp (MDHL) from Ophos instruments. The light emitted by the MDHL enters the ISAC chamber through a  $\text{MgF}_2$  window, and radiation is guided to the deposition substrate through a quartz tube inside the chamber. The UV-flux was measured at the end of the quartz tube with a calibrated Ni mesh to know the flux at the sample position (see González Díaz et al. 2019). Vacuum ultraviolet spectroscopy was carried out using a McPherson 0.2 m focal length UV monochromator (model 234/302) placed in front of the MDHL. The UV-absorption cross section of the ice samples was obtained applying eq. 2, where  $I_t(\lambda)$  is the transmitted intensity,  $I_0(\lambda)$  is the incident intensity,  $\sigma(\lambda)$  is the UV-absorption cross section of the ice, and  $N$  is the column density derived from the IR spectra, following Cruz-Díaz et al. (2014).

$$I_t(\lambda) = I_0(\lambda) \times e^{-\sigma(\lambda)N} \quad (2)$$

After ice irradiation, temperature programmed desorption (TPD) experiments were performed. A LakeShore 331 temperature controller connected to a silicon diode sensor with a sensibility better than 0.1 K was used to warm up the ice samples at 0.3 K/min up to 300 K. QMS data were recorded continuously and FTIR spectra were measured every 5 K during warm-up.

For  $\text{H}_2\text{O}:\text{CH}_3\text{OH}:\text{NH}_3$  experiments,  $\text{H}_2\text{O}$  and  $\text{CH}_3\text{OH}$  were introduced through the main gas line in ISAC, while  $\text{NH}_3$  was introduced through a second capillary tube, using a secondary gas line specifically designed for corrosive species.

## 2.2 IR spectra simulations

The calculation of the vibrational spectra for all the species collected in Fig. 2 has been done at the harmonic level using the well-tested Density Functional Theory hybrid method B3LYP. Different basis sets were used in exploratory calculations and finally the quadruple-z quality correlation consistent aug-cc-pVQZ, which includes both polarization and diffuse functions, was used for production purposes. Frequencies presented are not scaled and intensities are referred to the highest feature in each spectrum. All the calculations were carried out by means of Gaussian16 package (Frisch et al. 2016).

## 3 RESULTS AND DISCUSSION

### 3.1 Theoretical IR spectra

Fig. 2 shows the calculated IR spectra of three species related to HMT synthesis: TMT,  $\text{TMT}-(\text{CH}_2\text{OH})_3$  and HMT. The infrared spectra of TMT and  $\text{TMT}-(\text{CH}_2\text{OH})_3$  have, to our knowledge, not been reported before. The well known IR spectrum of HMT was also calculated to illustrate the reliability of the synthetic spectra. There is a good agreement between our measured IR spectrum of HMT and the calculated one, only the shift of the  $\text{CH}_x$  stretching modes near  $3000\text{ cm}^{-1}$ , also present in the calculated IR spectrum of HMT derivatives (Bera et al. 2019), is worth noting.

### 3.2 Effect of the ice environment over $\text{CH}_3\text{NH}_2$ ice.

Table 1 collects the different ice sample compositions, ice column density, and irradiation dose of the experiments presented in this work. Fig. 3 shows the methylamine IR features observed after deposition of  $\text{CH}_3\text{NH}_2$  molecules in different environments (Exp. 1, 5 and 6). Pure methylamine ice exhibits features (shown in Table 2) which are in good agreement with previous works (Durig et al. 1968; Zhu et al. 2019, and references therein). When  $\text{CH}_3\text{NH}_2$  is diluted in an inert matrix, Xe atoms in this work, intermolecular forces are reduced, and bands become narrower. N-H stretching vibrations ( $3500\text{--}3100\text{ cm}^{-1}$ ) seem to disappear in the Xe matrix, indicative of a large decrease of its IR band strength when molecules are isolated and H bonds are inhibited (Durig & Zheng 2001).  $\text{CH}_3\text{NH}_2$  in a  $\text{CH}_3\text{NH}_2:\text{H}_2\text{O}$  (1:1) ice mixture (Exp. 6) shows the same IR features observed for pure  $\text{CH}_3\text{NH}_2$  ice, slightly red-shifted by the different intermolecular forces present in this ice, and widened, as a consequence of the

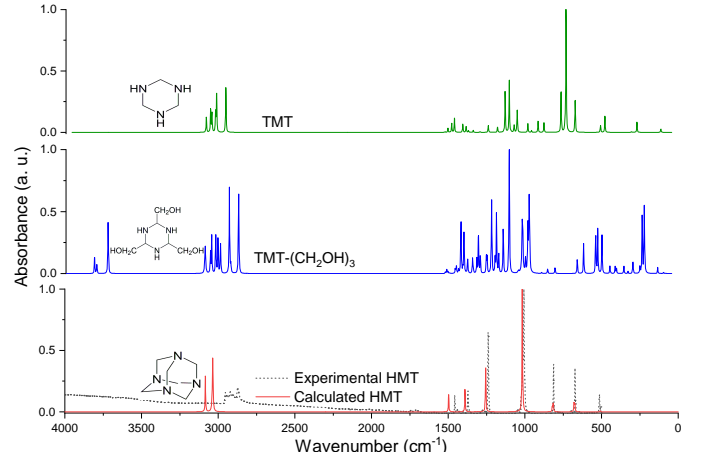


**Figure 2.** Calculated IR spectra of three species related to HMT synthesis: TMT,  $\text{TMT}-(\text{CH}_2\text{OH})_3$  and HMT itself. Dash black line shows the experimental IR spectra of HMT for comparison. Absorbance was normalized to 1 in all cases.

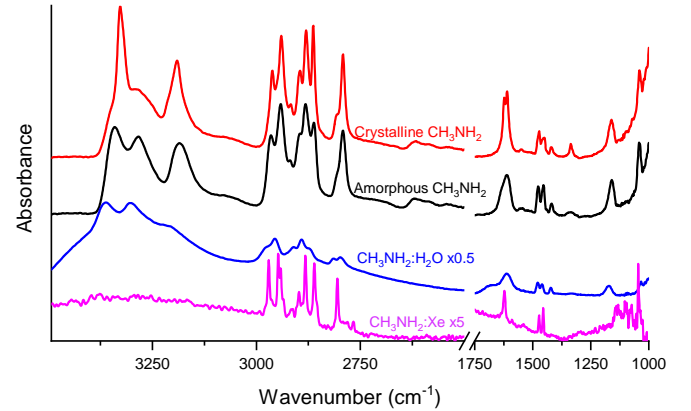


**Figure 3.** IR spectra recorded after deposition of different ice samples.  $\text{CH}_3\text{NH}_2:\text{Xe}$  (pink, Exp. 5),  $\text{CH}_3\text{NH}_2:\text{H}_2\text{O}$  (blue, Exp. 9), and pure  $\text{CH}_3\text{NH}_2$  at 8 K (black, Exp. 1) and 110 K (red, after crystallization process in Exp. 1). Band positions agree with those reported for pure  $\text{CH}_3\text{NH}_2$  ice (Durig et al. 1968; Zhu et al. 2019).

interaction of  $\text{CH}_3\text{NH}_2$  with  $\text{H}_2\text{O}$  neighbouring molecules. N-H stretching bands, however, are not weakened in a  $\text{H}_2\text{O}$  dominated ice. O-H groups in water ice can interact strongly with N-H groups, as both N and O atoms are able to establish hydrogen bonds.

TPD experiments over a non-irradiated  $\text{CH}_3\text{NH}_2$  ice revealed no major changes in the IR spectra up to 100 K. The onset of  $\text{CH}_3\text{NH}_2$  crystallization occurs near 100 K,  $\text{CH}_3\text{NH}_2$  acquires a crystalline structure (Fig. 3), ejecting molecules with a low-binding energy during this process. Fig. 4 shows the thermal desorption of  $\text{CH}_3\text{NH}_2$  in the different environments studied in this work. Pure methylamine ice sublimates from 100 K, having its maximum desorption at 142 K. The desorbed molecules are responsible for the QMS peak starting at 90 K with a maximum at 106 K in the Xe isolated methylamine ice (middle panel of Fig. 4). When Xe atoms thermally desorb at 66 K, the remaining methylamine molecules do not strongly interact. Intermolecular forces are reduced, and thermal desorption takes place at lower temperature corresponding to the onset temperature of desorption in the pure  $\text{CH}_3\text{NH}_2$  ice

**Table 1.** Experiments performed in this work

Exp.	Ice sample	$N_0$ ( $\text{CH}_3\text{NH}_2$ ) ( $\text{cm}^{-2}$ )	Photon dose	
			Absolute ( $\text{cm}^{-2}$ )	per molecule ( $\text{cm}^{-2}$ )
1	$\text{CH}_3\text{NH}_2$	$2.4 \times 10^{17}$	0	0
2	$\text{CH}_3\text{NH}_2$	$3.2 \times 10^{17}$	$1.0 \times 10^{18}$	3.2
3	$\text{CH}_3\text{NH}_2$	$6.1 \times 10^{17}$	$1.4 \times 10^{18}$	2.5
4	$\text{CH}_3\text{NH}_2$	$1.2 \times 10^{18}$	$1.5 \times 10^{18}$	1.1
5	$\text{CH}_3\text{NH}_2:\text{Xe}^{**}$	$2.2 \times 10^{16}$	$1.0 \times 10^{18}$	-
6	$\text{CH}_3\text{NH}_2:\text{H}_2\text{O}$ (1:1)	$3.9 \times 10^{17}$	$9.0 \times 10^{17}$	1.2
7	$\text{CH}_3\text{NH}_2:\text{H}_2\text{O}^*$ (2:1)	$6.0 \times 10^{17}$	$2.7 \times 10^{18}$	1.5
8	$\text{CH}_3\text{NH}_2$	$1.9 \times 10^{19}$	$3.6 \times 10^{19}$	1.9
9	$\text{CH}_3\text{NH}_2:\text{H}_2\text{O}$ (1:2)	$2.0 \times 10^{18}$	$1.5 \times 10^{18}$	0.25

\* Experiment 7 was irradiated during the warm-up, between 8 K and 110 K. This irradiation represents the 40% of the total photon dose.

\*\* Absorption of Xe atoms prevented us from the quantification of methylamine photon dose, see Fig. 5.

**Table 2.** IR features of  $\text{CH}_3\text{NH}_2$  in the different ice mixtures. For pure  $\text{CH}_3\text{NH}_2$  ice, data agree with Durig et al. (1968); Zhu et al. (2019). For  $\text{CH}_3\text{NH}_2:\text{Xe}$  and  $\text{CH}_3\text{NH}_2:\text{H}_2\text{O}$ , no reference was found in the literature.

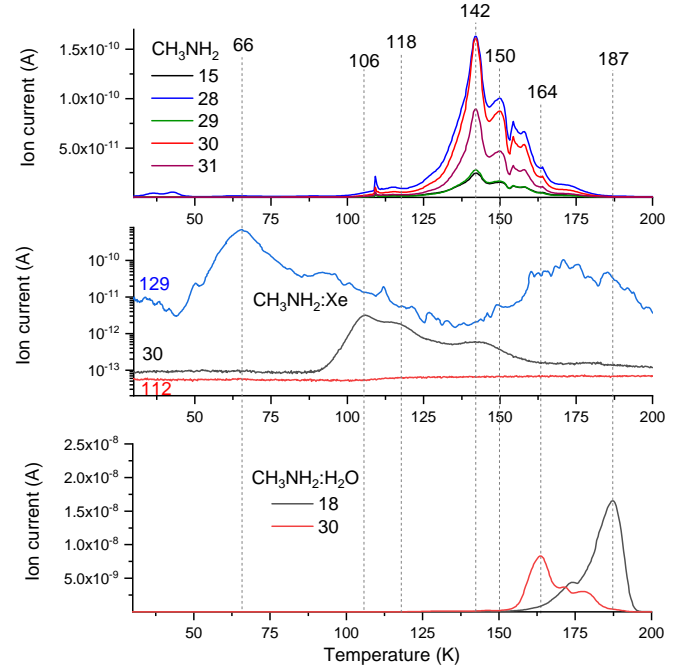
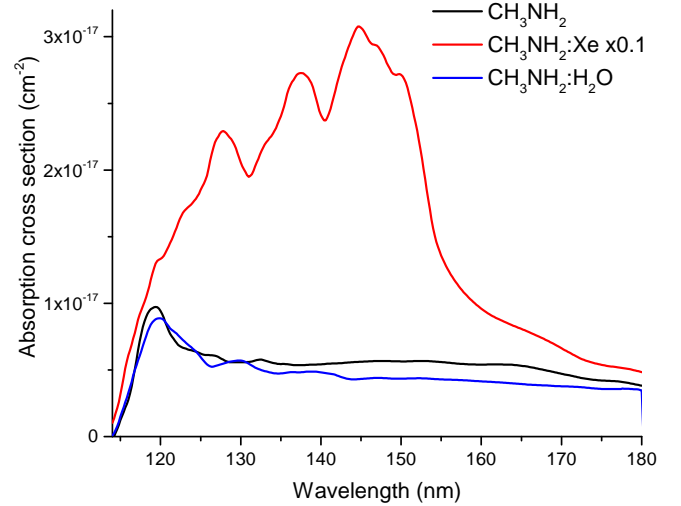
Vibration mode	$\text{CH}_3\text{NH}_2:\text{Xe}$	$\text{CH}_3\text{NH}_2$	$\text{CH}_3\text{NH}_2:\text{H}_2\text{O}$
$\text{NH}_2$ antisymmetric str.	-	3347	3354
$\text{NH}_2$ symmetric str.	-	3286	3286
H bonding	-	3182	3186
$\text{CH}_3$ degenerate str.	2970, 2942	2968, 2944	2968, 2945
$\text{CH}_3$ degenerate str.	2882, 2861	2884, 2864	2919, 2878
$\text{CH}_3$ symmetric str.	2805, 2766	2808, 2793	2809, 2792
$\text{NH}_2$ scissoring	1622	1613	1612
$\text{CH}_3$ degenerate bend	1472, 1455	1476, 1457	1478, 1457
$\text{NH}_2$ twist	-	1418	1421
-	-	1337	-
$\text{CH}_3$ rocking	-	1161	1166
C-N str.	1045	1041	1040
$\text{NH}_2$ wagging	-	995	-

str. = stretching; bend. = bending

shown in the top panel of Fig. 4. Co-deposition with less-volatile  $\text{H}_2\text{O}$  molecules delays  $\text{CH}_3\text{NH}_2$  thermal desorption to 164 K. Indeed, some methylamine molecules remain in the solid phase at larger temperatures, desorbing during the crystallization of  $\text{H}_2\text{O}$  molecules, around 175 K. From Fig. 4, it can be concluded that methylamine thermal desorption is strongly dependent on its environment, as it happens with the type of substrate when dealing with monolayer-thick ices (Chaabouni et al. 2018).

### 3.3 UV irradiation of $\text{CH}_3\text{NH}_2$ ice samples. $\text{H}_2$ formation and diffusion. Saturation of species

As it can be seen in Table 1, the column density of  $\text{CH}_3\text{NH}_2$  in the pure ice samples was larger by a factor of  $\geq 10$  compared to  $\text{CH}_3\text{NH}_2:\text{Xe}$  ice sample (Exps. 2 and 6). From the UV absorption cross section of methylamine presented in Fig. 5, and using eq. 2, a column density of  $6.9 \times 10^{17} \text{ cm}^{-2}$  corresponds to about 95% UV absorption for pure methylamine ice, and  $4.2 \times 10^{17} \text{ cm}^{-2}$  for a

**Figure 4.** Top: thermal desorption of unirradiated  $\text{CH}_3\text{NH}_2$  ice leading to ejection of these molecules to the gas phase. The most intense  $\frac{m}{z}$  fragments of  $\text{CH}_3\text{NH}_2$  are recorded. Middle: thermal desorption of Xe and  $\text{CH}_3\text{NH}_2$  during warm-up of experiment 6. No signal is expected for  $\frac{m}{z} = 112$ , it is shown for comparison. Bottom: thermal desorption of  $\text{CH}_3\text{NH}_2$  and  $\text{H}_2\text{O}$  during warming up of experiment 10.**Figure 5.** UV spectra of pure  $\text{CH}_3\text{NH}_2$  (black trace),  $\text{CH}_3\text{NH}_2:\text{Xe}$  (red trace), and  $\text{CH}_3\text{NH}_2:\text{H}_2\text{O}$  (blue trace) ice samples. Note that Xe atoms dominate the UV absorption in the  $\text{CH}_3\text{NH}_2:\text{Xe}$  ice sample, see text.

95% UV absorption in the  $\text{CH}_3\text{NH}_2:\text{Xe}$  ice sample. Therefore, in our experiments, most of the  $\text{CH}_3\text{NH}_2$  molecules in the ice were exposed to UV radiation. UV-thick ices were irradiated during the deposition process, their corresponding photon dose is shown in Table 1. The large difference between  $\text{CH}_3\text{NH}_2$  (both pure and in  $\text{H}_2\text{O}$  mixture) with the UV spectrum of  $\text{CH}_3\text{NH}_2:\text{Xe}$  ice mixture (see Fig. 5) is due to the UV absorption of Xe ice, in line with the

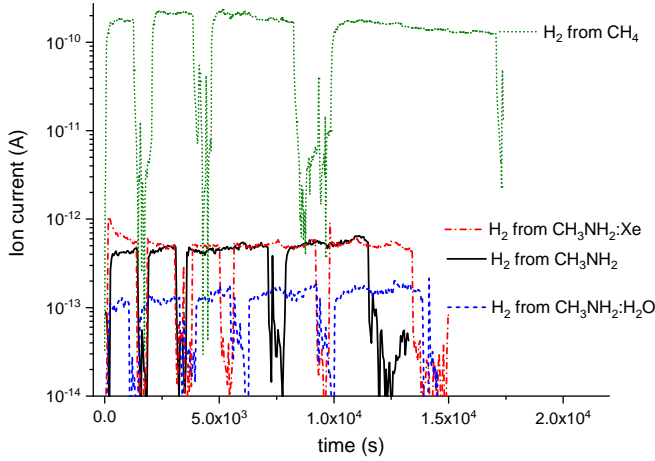


**Figure 6.**  $\text{H}_2$  signal recorded during irradiation of  $\text{CH}_3\text{NH}_2$  pure (Exp. 2),  $\text{CH}_3\text{NH}_2:\text{Xe}$  (Exp. 5), and  $\text{CH}_3\text{NH}_2:\text{H}_2\text{O}$  (Exp. 7) ice samples.  $\text{H}_2$  signal from irradiation of  $\text{CH}_4$  ice is shown for comparison (Carrascosa et al. 2020). Fast changes between the larger and the lower  $\text{H}_2$  signal are produced when the UV lamp is turned on and off along the irradiation period. Horizontal lines are drawn to guide the eye. Note that the y-axis is in logarithmic scale.

Xe absorption presented by Schnepp & Dressler (1960).

H $\cdot$  subtraction is the main process concerning UV irradiation of methylamine. The high mobility of hydrogen atoms in the ice bulk and surface allows the fast formation of  $\text{H}_2$  molecules. Diffusion and eventual ejection of  $\text{H}_2$  molecules enables its detection by QMS, where a larger signal is expected for the pure  $\text{CH}_3\text{NH}_2$  ice when compared to  $\text{CH}_3\text{NH}_2:\text{Xe}$  ice mixture, due to its larger  $\text{CH}_3\text{NH}_2$  column density. Nevertheless, Fig. 6 shows that ion current measured for  $\frac{m}{z} = 2$ , related to desorbing  $\text{H}_2$  molecules is similar in both experiments. The formation of hydrogen bonds in the ice avoids hydrogen diffusion. Therefore, pure  $\text{CH}_3\text{NH}_2$  ice shows a lower  $\text{H}_2$  diffusion compared to matrix isolated  $\text{CH}_3\text{NH}_2$ . The addition of  $\text{H}_2\text{O}$  allows the formation of more hydrogen bonds, reducing  $\text{H}_2$  diffusion even further. A lower  $\text{H}_2$  diffusion makes H $\cdot$  atoms and  $\text{H}_2$  molecules remain longer in the  $\text{CH}_3\text{NH}_2$  and the  $\text{CH}_3\text{NH}_2:\text{H}_2\text{O}$  ice samples, enhancing chemical reactions with  $\cdot\text{CH}_2\text{NH}_2$  and  $\text{CH}_3\text{NH}\cdot$  radicals to form back  $\text{CH}_3\text{NH}_2$ . This recombination leads to a lower than expected  $\text{H}_2$  signal in the QMS (Fig. 6), as well as to a lower overall dissociation of  $\text{CH}_3\text{NH}_2$  molecules during UV irradiation, shown in Fig. 7. In the  $\text{CH}_3\text{NH}_2:\text{Xe}$  ice samples, hydrogen diffusion is larger, and recombination is quenched.

### 3.4 UV irradiation of $\text{CH}_3\text{NH}_2$ , $\text{CH}_3\text{NH}_2:\text{Xe}$ and $\text{CH}_3\text{NH}_2:\text{H}_2\text{O}$ ice samples. Photoproducts formation.

IR spectra measured during the irradiation period of  $\text{CH}_3\text{NH}_2$ ,  $\text{CH}_3\text{NH}_2:\text{Xe}$  and  $\text{CH}_3\text{NH}_2:\text{H}_2\text{O}$  ice samples (Exps. 2, 6 and 7) are shown in Fig. 8, and Table 3 exhibits the assignment of the IR bands. Fig. 9 summarizes the different species arising from UV irradiation at 8 K. The formation of different species at low temperature is presented starting from the simplest ice sample,  $\text{CH}_3\text{NH}_2:\text{Xe}$  to the most astrophysically relevant one,  $\text{CH}_3\text{NH}_2:\text{H}_2\text{O}$ . Pure  $\text{CH}_3\text{NH}_2$  ice sample served as an intermediate step.

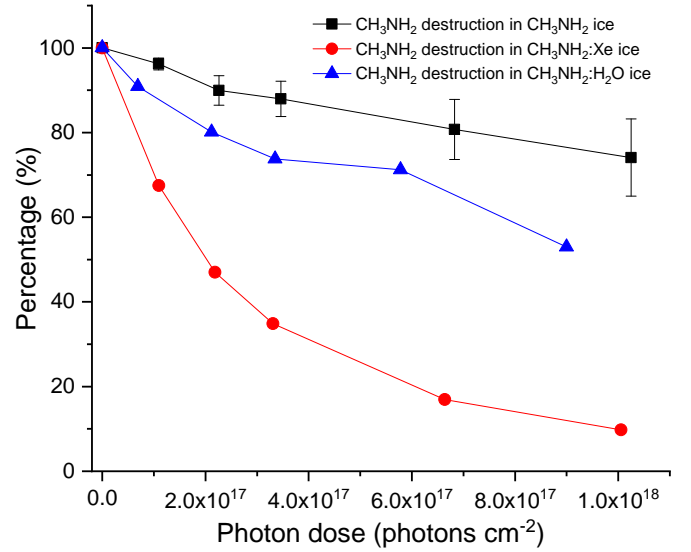


**Figure 7.** Decrease in the  $\text{CH}_3\text{NH}_2$  column density after each irradiation interval for  $\text{CH}_3\text{NH}_2$  (Exp. 2),  $\text{CH}_3\text{NH}_2:\text{Xe}$  (Exp. 5) and  $\text{CH}_3\text{NH}_2:\text{H}_2\text{O}$  (Exp. 7).

#### 3.4.1 UV irradiation of $\text{CH}_3\text{NH}_2:\text{Xe}$ ice samples

IR spectra during the irradiation of  $\text{CH}_3\text{NH}_2:\text{Xe}$  ice samples is shown in Fig. 8a. Matrix isolation of methylamine enhances the detection of radical species.  $\cdot\text{NH}_2$  was detected by its IR feature at  $1500\text{ cm}^{-1}$ , in line with the position of this radical formed from UV irradiation of  $\text{NH}_3$  (Martín-Doménech et al. 2018). The large hydrogen subtraction hampers the formation of hydrogenated species.  $\text{NH}_3$  was, in fact, not detected at 8 K, although the low N-H stretching band strength at low temperature may hinder its detection.  $\text{CH}_4$ , which can be formed by direct decomposition of methylamine molecules at wavelengths shorter than 388 nm (Gardner & McNesby 1982), was detected as a minor photoproduct. Furthermore,  $\text{CH}_3\cdot$  radicals present in the  $\text{CH}_3\text{NH}_2:\text{Xe}$  ice mixture can only react with H $\cdot$  radicals of  $\text{H}_2$  molecules, as they are the only species able to move fast enough at 8 K, thus enhancing  $\text{CH}_4$  formation.

According to Bossa et al. (2012),  $\text{CH}_3\text{NH}\cdot$  and  $\cdot\text{CH}_2\text{NH}_2$  radicals are also expected to form directly from methylamine upon UV irradiation. The former was detected by its  $1025\text{ cm}^{-1}$  IR feature, while the latter was not identified, probably as a consequence of its lower formation rate (Bossa et al. 2012). Additionally, even if  $\cdot\text{CH}_2\text{NH}_2$  is formed, it tends to react, either with  $\cdot\text{CH}_3$  radicals to form ethylamine,  $\text{CH}_3\text{CH}_2\text{NH}_2$ , or losing a hydrogen atom to form  $\text{CH}_2\text{NH}$ . Nitrogen atoms, however, can stabilize the electron, thus reducing the reactivity of R-NH $_x$  radicals.

UV irradiation of matrix isolated methylamine led, preferentially, to the formation of  $\text{CH}_2\text{NH}$  molecules by hydrogen subtraction from methylamine. As reported by Gardner & McNesby (1982), the dissociation of  $\text{CH}_3\text{NH}_2$  molecules producing  $\text{CH}_2\text{NH}$  and  $\text{H}_2$  is the most energetically favoured process concerning UV irradiation of methylamine in the gas phase. Alternatively,  $\text{CH}_2\text{NH}$  can be obtained from hydrogen elimination from  $\text{CH}_3\text{NH}\cdot$  and  $\cdot\text{CH}_2\text{NH}_2$  radicals. Methyleneimine was detected through its IR features at  $3193, 3160, 2219, 1651, 1113$ , and  $1059\text{ cm}^{-1}$ .  $\text{CH}_2\text{NH}$  molecules can also undergo hydrogen subtraction. Thus, HCN

**Table 3.** New IR features (in  $\text{cm}^{-1}$ ) arising in the sample spectra during irradiation of the different ice mixtures at 8 K.

Mass	Species	Vibration mode	$\text{CH}_3\text{NH}_2:\text{Xe}$	$\text{CH}_3\text{NH}_2$ (5% $\text{H}_2\text{O}$ )	$\text{CH}_3\text{NH}_2:\text{H}_2\text{O}$	Reference
16	$\text{CH}_4$	C-H str.	3010	3013	3005	D'Hendecourt et al. (1986)
16	$\text{CH}_4$	C-H bend.	1301	1303	1306	D'Hendecourt et al. (1986)
16	$\text{NH}_2^-$	N-H bend.	1500	-	-	Bossa et al. (2012)
17	$\text{NH}_3$	N-H str.	-	3390	3405	Ferraro et al. (1980); Danger et al. (2011a)
17	$\text{NH}_3$	umbrella mode	-	1070	1076	Ferraro et al. (1980); Danger et al. (2011a)
26	$\text{CN}^-$	$\text{C}\equiv\text{N}$ str.	2084	2069	2080	Moore & Hudson (2003); Danger et al. (2011b)
27	$\text{HNC}$	N-H str.	3576	-	-	Jacox & Milligan (1975); Moore & Hudson (2003); Mencos & Krim (2018)
27	$\text{HCN}$	C-H str.	3277	-	-	Jacox & Milligan (1975); Moore & Hudson (2003); Mencos & Krim (2018)
27	$\text{HCN}$	$\text{C}\equiv\text{N}$ str.	2133	-	-	Moore & Hudson (2003); Mencos & Krim (2018)
29	$\text{CH}_2\text{NH}$	$\text{CH}_2$ degenerate str.	3193, 3160	-	-	Zhu et al. (2019)
29	$\text{CH}_2\text{NH}$	comb.	2219	-	-	Danger et al. (2011b)
29	$^*\text{CH}_2\text{NH}$	$\text{C}=\text{N}$ str.	1651	-	-	Jacox & Milligan (1975); Danger et al. (2011b); Zhu et al. (2019)
29	$\text{CH}_2\text{NH}$	C-N torsion	1105	1119	-	Jacox & Milligan (1975)
29	$\text{CH}_2\text{NH}$	$\text{HCNH}$ def.	1059	1068	-	Jacox & Milligan (1975)
30	$\text{H}_2\text{CO}$	C-H str.	-	2828	2830	Schutte et al. (1993); Vinogradoff et al. (2012)
30	$\text{H}_2\text{CO}$	C=O str.	-	1718	1729	Schutte et al. (1993); Vinogradoff et al. (2012)
30	$\text{H}_2\text{CO}$	$\text{CH}_2$ bend.	-	1498	1493	Schutte et al. (1993); Vinogradoff et al. (2012)
30	$^*\text{CH}_2\text{NH}_2$	N-H str.	-	3450-3380	-	Dyke et al. (1989)
30	$\text{CH}_3\text{NH}$	comb.	1025	-	-	Ruzi & Anderson (2012)
32	$\text{CH}_3\text{NH}_3^+$	comb.	-	2654	2645	Bossa et al. (2009a); Bossa et al. (2012)
32	$\text{CH}_3\text{NH}_3^+$	comb.	-	2553	2552	Bossa et al. (2009a); Bossa et al. (2012)
41	$\text{CH}_3\text{CN}$	$\text{C}\equiv\text{N}$ str.	2255	2254	-	Wexler (1967); D'Hendecourt et al. (1986); Danger et al. (2011a)
42	$\text{OCN}^-$	$\text{C}\equiv\text{N}$ str.	-	2156	2162	Moore & Hudson (2003); Jiménez-Escobar et al. (2014)
43	$\text{CH}_3\text{CHNH}$	C=N str.	-	1668	1679	Stolkin et al. (1977); Danger et al. (2011a)
43	$\text{CH}_3\text{CHNH}$	$\text{CH}_3$ bend.	-	1438	1442	Stolkin et al. (1977); Danger et al. (2011a)
45	$\text{HCONH}_2$	$\text{NH}_2$ scissoring	-	1635	1636	Sivaraman et al. (2013)
45	$\text{HCONH}_2$	CH bend.	-	1386	1384	Sivaraman et al. (2013)
45	$\text{CH}_3\text{CH}_2\text{NH}_2$	N-H str.	-	3308	3323	Danger et al. (2011a)
45	$\text{CH}_3\text{CH}_2\text{NH}_2$	N-H str.	-	3219	3236	Danger et al. (2011a)
45	$\text{CH}_3\text{CH}_2\text{NH}_2$	N-H str.	-	3104	3121	Danger et al. (2011a)
45	$\text{CH}_3\text{CH}_2\text{NH}_2$	C-C-N str.	-	1095	-	Durig et al. (2006); Danger et al. (2011a)
?	?		1339	-	-	
?	?		1589	-	-	

str. = stretching; bend. = bending; def. = deformation

\* tentatively assigned.

molecules are obtained. HCN was detected by its IR features at  $3277\text{ cm}^{-1}$  and  $2133\text{ cm}^{-1}$  (see Table 3). HNC molecules, which are far less stable than its HCN isomer, were also detected by its IR feature at  $3576\text{ cm}^{-1}$  (Fig. 8a). As reported by Milligan & Jacox (1967), HNC formation is enhanced in a matrix environment. The absorption at  $2084\text{ cm}^{-1}$  is indicative of the presence of cyanide,  $\text{CN}^-$ , species, although it could not be attributed to any specific salt.

As depicted in Table 3, UV irradiation of  $\text{CH}_3\text{NH}_2:\text{Xe}$  ice samples promotes the formation of small species, which can be produced from just one parent  $\text{CH}_3\text{NH}_2$  molecule.  $\text{CH}_3\text{CN}$ , tentatively detected in isolated methylamine UV irradiation, was the only species that involves reaction of two  $\text{CH}_3\text{NH}_2$  molecules. Indeed,  $\text{CH}_3\text{CN}$  was only detected in an advanced stage of the irradiation period, suggesting the reduced mobility of radicals at 8 K.

#### 3.4.2 UV irradiation of pure $\text{CH}_3\text{NH}_2$ ice samples

IR spectra of a pure  $\text{CH}_3\text{NH}_2$  ice sample is represented in Fig. 8b.  $\text{CH}_3\text{NH}_2$ ,  $\cdot\text{CH}_2\text{NH}_2$ ,  $\cdot\text{CH}_3$  and  $\cdot\text{NH}_2$  radicals can be directly obtained from UV irradiation of methylamine (Bossa et al. 2012). In the pure  $\text{CH}_3\text{NH}_2$  ice sample, radicals bearing NH groups appear as broad bands at both sides of the N-H stretching region of the IR spectrum. In line with Martín-Doménech et al. (2018), radicals appear readily within the irradiation period, but they are

readily consumed, keeping a constant formation and destruction rate for longer irradiation times.

The lower hydrogen diffusion in the pure  $\text{CH}_3\text{NH}_2$  ice, compared to matrix isolated methylamine, is expected to produce a larger fraction of hydrogenated species, such as  $\text{NH}_3$  and  $\text{CH}_4$ .  $\text{NH}_3$  and  $\text{CH}_4$  were, in fact, detected in  $\text{CH}_3\text{NH}_2$  ice samples (see Table 3 and Fig. 8b). Martín-Doménech et al. (2018) demonstrated that  $\text{NH}_2\cdot$  radicals can remain in a pure  $\text{NH}_3$  ice until thermal energy enables chemical reactions. Indeed,  $\text{NH}_2\cdot$  radicals can only react with hydrogen atoms at 8 K to form  $\text{NH}_3$  molecules in methylamine ice, explaining the plateau reached in  $\text{NH}_2\cdot$  formation in Martín-Doménech et al. (2018). The low absorbance at  $1303$  and  $3013\text{ cm}^{-1}$  is indicative of a minor formation rate of  $\text{CH}_4$  in pure  $\text{CH}_3\text{NH}_2$  ice samples. Irradiation of pure methane ice also produces  $\text{CH}_3\cdot$  radicals, which react very readily to form small hydrocarbons and hydrogenated amorphous carbon, even at 8 K (Carrascosa et al. 2020, and references therein). As it will be explained later on, IR spectra from pure  $\text{CH}_3\text{NH}_2$  ice displays ethylamine ( $\text{CH}_3\text{CH}_2\text{NH}_2$ ), ethylenimine ( $\text{CH}_3\text{CHNH}$ ) and acetonitrile ( $\text{CH}_3\text{CN}$ ) IR features. The formation of many  $\text{CH}_3\cdot$ -bearing species suggests that  $\text{CH}_3\cdot$  radicals are more prone to react with other species rather than  $\text{H}\cdot$  radicals, as it occurs in the  $\text{CH}_4$  ice UV irradiation experiments (Carrascosa et al. 2020). Despite the fast formation of ethane and propane, these authors showed that the reaction  $\text{CH}_3\cdot + \text{H}\cdot \rightarrow \text{CH}_4$  is not efficient, at least in the ice surface. As a consequence, the interaction of  $\text{H}\cdot$  radicals

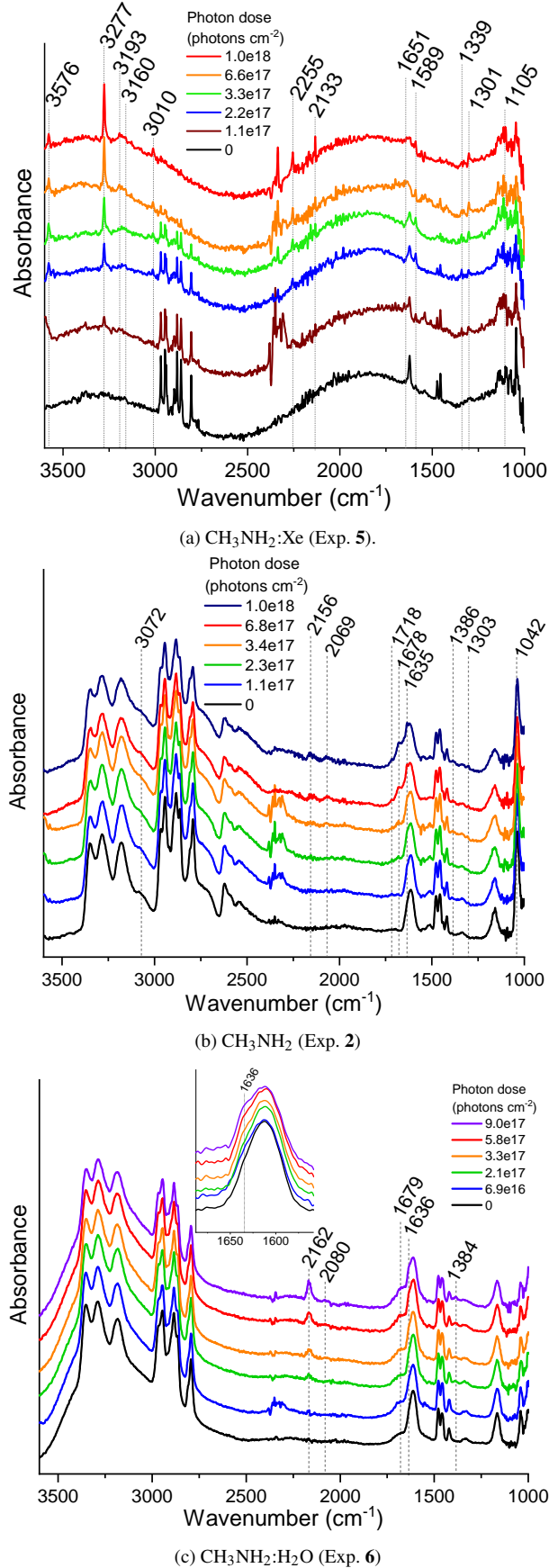


**Figure 8.** Evolution of the IR spectra during the irradiation of three different ice samples. Vertical lines indicate the most relevant changes. The vibrational and molecular assignments are provided in Table 3.

in  $\text{CH}_4$  ice is small and  $\text{H}_2$  desorption is 100 times larger in a pure  $\text{CH}_4$  ice than the one found in  $\text{CH}_3\text{NH}_2$  ice in our experiments for similar ice thicknesses (Fig. 6).

$\text{CH}_3\cdot$  and  $\cdot\text{CH}_2\text{NH}_2$  radicals will react leading to an efficient formation of ethylamine. Ethylamine IR features overlap with those of methylamine. Yet, the relative intensity between the symmetric and the antisymmetric N-H stretching modes (Hashiguchi et al. 1984; Danger et al. 2011a) allowed us to infer its presence. The difference spectra between the irradiated and the non-irradiated methylamine ice (shown in Fig. 10) confirmed the presence of ethylamine by its IR features at 3308, 3219, 3104 and  $1095\text{ cm}^{-1}$  (see Table 3).

$\text{CH}_2\text{NH}$  was tentatively detected in pure  $\text{CH}_3\text{NH}_2$  ice by its IR bands at 1119 and  $1068\text{ cm}^{-1}$ . The presence of other molecules and radicals around  $\text{CH}_2\text{NH}$  molecules enhance its reactivity, lowering its abundance with respect to matrix isolated methylamine. Methyleneimine reaction with  $\text{CH}_3\cdot$  radicals produces ethylenimine ( $\text{CH}_3\text{CHNH}$ ), which was detected by its IR features at  $1438\text{ cm}^{-1}$  and  $1668\text{ cm}^{-1}$ . Dehydrogenation of  $\text{CH}_3\text{CHNH}$  molecules produces  $\text{CH}_3\text{CN}$ , responsible of the IR band at  $2254\text{ cm}^{-1}$ . Dehydrogenation of  $\text{CH}_2\text{NH}$  molecules produces hydrogen cyanide, HCN. HCN molecules were not detected in pure  $\text{CH}_3\text{NH}_2$  ice samples, but  $\text{CN}^-$  anions were. As reported by Bossa et al. (2012), HCN and surrounding  $\text{CH}_3\text{NH}_2$  molecules give rise to methylammonium cyanide [ $\text{CH}_3\text{NH}_3^+ \text{CN}^-$ ] salt, detected in the IR spectra by the IR features at 2654 and  $2553\text{ cm}^{-1}$  from the cation and  $2069\text{ cm}^{-1}$  from the anion (see Table 3 and Fig. 8b). This reaction is favoured by the formation of  $\text{CH}_3\text{NH}_3^+$  cation (Zhang et al. 2017), which explains the lower formation rate of  $\text{CN}^-$  in the  $\text{CH}_3\text{NH}_2:\text{Xe}$  experiment. The formation of other cyanides, however, cannot be excluded, with IR bands overlapping in the  $2069\text{ cm}^{-1}$  feature.

When referring to pure methylamine ice, we assume that some  $\text{H}_2\text{O}$  molecules ( $\approx 5\%$ ) are present, due to the deposition process, as explained in Sect. 2. Although  $\text{CH}_3\text{NH}_2$  vapour pressure is higher than that of  $\text{H}_2\text{O}$ , it is not possible to get rid of all the  $\text{H}_2\text{O}$ . Therefore, some oxygenated compounds were detected from UV irradiation of  $\text{CH}_3\text{NH}_2$  ice. Chemical reactions between  $\text{CH}_2\text{NH}$  and OH radicals (formed from UV irradiation of  $\text{H}_2\text{O}$  molecules) are shown in Fig. 11. The nucleophilic attack of an OH radical over a carbon atom in a methylenimine molecule leads to the formation of aminomethanol as an intermediate. Formamide,  $\text{HCONH}_2$ , formation has been reported at low temperature during UV irradiation of aminomethanol ice through radical reactions (Bossa et al. 2009b). Additionally, the nucleophilic attack by the alcohol group over the aminomethanol intermediate results in formamide formation in a barrier-less reaction, as reported by Vazart et al. (2016). Martín-Doménech et al. (2020) reported the formation of formamide from radical reaction between  $\text{NH}_2$  and HCO radicals, although the relatively low formation rate of these radicals in  $\text{CH}_3\text{NH}_2:\text{H}_2\text{O}$  ice samples suggests a negligible formation through this mechanism in our experiments. Formamide was identified by its  $1386\text{ cm}^{-1}$  and  $1635\text{ cm}^{-1}$  IR features in Fig. 8b and Table 3 (note that the  $1635\text{ cm}^{-1}$  band is observed as a contribution to the left shoulder of the prominent band around  $1610\text{ cm}^{-1}$ ). These features display a weak intensity but they were highly reproducible in our experiments. As shown in Fig. 11, elimination of the amino group during the second nucleophilic attack results in formaldehyde,  $\text{H}_2\text{CO}$ , detected in the IR spectrum

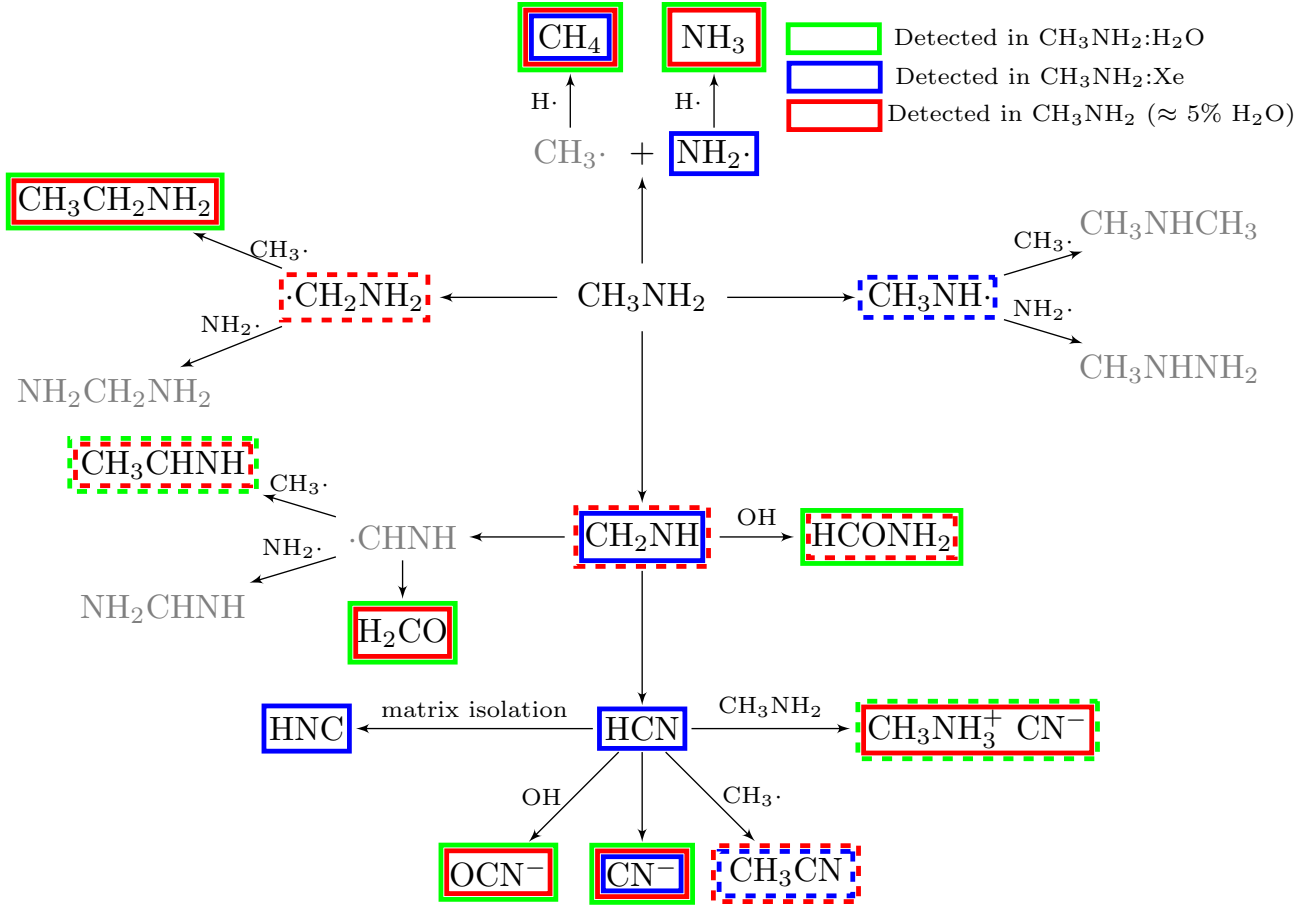


**Figure 9.** Species arising from UV irradiation at 8 K of different ice samples containing  $\text{CH}_3\text{NH}_2$ . Colours are indicative of species found in  $\text{CH}_3\text{NH}_2:\text{H}_2\text{O} = 100:5$  (red),  $\text{CH}_3\text{NH}_2:\text{Xe}$  (blue), and  $\text{CH}_3\text{NH}_2:\text{H}_2\text{O} = 1:1$  (green) ice samples. Light grey denote non-detected species, which require the reaction of, at least, one  $\text{NH}_x$  group, less reactive than methyl groups, see Sect. 3.3. Dashed lines are indicative of a tentative detection, from reproducible bands which are close to the detection limit. Identification of the different species was made by the following IR features, some were also detected during thermal desorption by QMS:  $\text{CH}_4$ , bands at 1303 and 3013  $\text{cm}^{-1}$ ;  $\text{NH}_3$ , 3390  $\text{cm}^{-1}$ ;  $\text{NH}_2\cdot$ , decay of the N-H bending mode around 1500  $\text{cm}^{-1}$ ;  $\cdot\text{CH}_2\text{NH}_2$ , decay of N-H stretching around 3400  $\text{cm}^{-1}$ ;  $\text{CH}_3\text{CH}_2\text{NH}_2$ , bands near 3308, 3219, 3104, and 1095  $\text{cm}^{-1}$  after subtraction between irradiated and non-irradiated ice samples;  $\text{CH}_3\text{NH}\cdot$ , 1025  $\text{cm}^{-1}$  feature in Xe matrix;  $\text{CH}_2\text{NH}$ , bands at 3193, 3160, 2219, 1105, and 1059  $\text{cm}^{-1}$ ;  $\text{HCONH}_2$ , 1635 and 1386  $\text{cm}^{-1}$  and thermal desorption at 205 K ( $\frac{m}{z} = 45$ );  $\text{H}_2\text{CO}$ , bands at 2828 and 1718  $\text{cm}^{-1}$ ;  $\text{CH}_3\text{CHNH}$ , bands at 1668, 1438  $\text{cm}^{-1}$ , and thermal desorption at 200 K ( $\frac{m}{z} = 45$ );  $\text{HCN}$ , bands at 3277, and 2133  $\text{cm}^{-1}$ , thermal desorption at 114 K ( $\frac{m}{z} = 27$ );  $\text{HNC}$ , 3576  $\text{cm}^{-1}$  band and thermal desorption at 105 K ( $\frac{m}{z} = 27$ );  $\text{OCN}^-$ , 2156  $\text{cm}^{-1}$ ;  $\text{CN}^-$ , 2069  $\text{cm}^{-1}$ ;  $\text{CH}_3\text{CN}$ , 2254  $\text{cm}^{-1}$ ;  $\text{CH}_3\text{NH}_3^+ \text{CN}^-$ , 2654, 2553, and 2069  $\text{cm}^{-1}$ .

by its C=O stretching absorption at 1718  $\text{cm}^{-1}$ , and ammonia formation (Layer 1963). Furthermore, dehydration of formamide produces  $\text{HNCO}$ , which readily undergoes hydrogen subtraction in presence of  $\text{CH}_3\text{NH}_2$  to produce  $\text{OCN}^-$  anions, detected by its main IR feature at 2156  $\text{cm}^{-1}$ , and  $\text{CH}_3\text{NH}_3^+$  cations. The relatively large band strengths of oxygenated compounds facilitate their detection, even when  $\text{H}_2\text{O}$  is a minor compound in the ice sample.

### 3.4.3 UV irradiation of pure $\text{CH}_3\text{NH}_2:\text{H}_2\text{O}$ ice samples

The presence of methylamine was inferred in comet 67P/Churyumov-Gerasimenko and this species was detected in the gas phase toward molecular clouds and hot cores, see Sect. 1 (Goesmann et al. 2015). Pure methylamine ice, however, is not a good analog of astrophysical ices. Thus, more astrophysically realistic  $\text{H}_2\text{O}:\text{CH}_3\text{NH}_2$  ice experiments were performed. The

understanding of the processes in  $\text{CH}_3\text{NH}_2:\text{Xe}$  and pure  $\text{CH}_3\text{NH}_2$  ice samples was, however, found to be crucial to understand the processes going on in this binary ice mixture.

$\text{CH}_3\text{NH}_2:\text{H}_2\text{O}$  ice mixtures were prepared at different ratios between the components (see Table 1). Fig. 8c shows the evolution of the IR spectra of Exp. 6, where a column density of  $3.9 \times 10^{17} \text{ cm}^{-2}$  and  $3.5 \times 10^{17} \text{ cm}^{-2}$  for  $\text{CH}_3\text{NH}_2$  and  $\text{H}_2\text{O}$ , respectively, was measured.

The presence of OH groups raises the reactivity of radicals within the  $\text{CH}_3\text{NH}_2:\text{H}_2\text{O}$  ice sample, in comparison to pure  $\text{CH}_3\text{NH}_2$  and  $\text{CH}_3\text{NH}_2:\text{Xe}$ , preventing from the detection of radical species. The formation of ethylamine,  $\text{CH}_3\text{CH}_2\text{NH}_2$  (IR bands at 3323, 3236 and 3121  $\text{cm}^{-1}$ ) is indicative of the presence of  $\cdot\text{CH}_2\text{NH}_2$  and  $\cdot\text{CH}_3$  radicals, as it occurs in the pure  $\text{CH}_3\text{NH}_2$  ice sample. IR bands at 3005 and 1306  $\text{cm}^{-1}$  ( $\text{CH}_4$ ) and 3405 and 1076  $\text{cm}^{-1}$  ( $\text{NH}_3$ ), confirm the enhanced formation of these

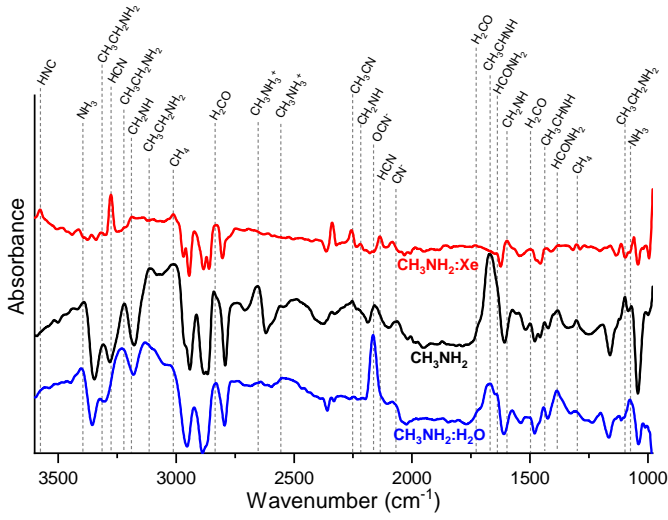


**Figure 10.** IR spectra of irradiated  $\text{CH}_3\text{NH}_2:\text{Xe}$  (red),  $\text{CH}_3\text{NH}_2$  (black) and  $\text{CH}_3\text{NH}_2:\text{H}_2\text{O}$  (blue) ice mixtures after subtraction of the corresponding non-irradiated IR spectra.

species when hydrogen bonds are established.

Although the highly reactive  $\text{CH}_2\text{NH}$  was not identified, its presence as an intermediate species can be inferred by the presence of IR bands at  $1636$  and  $1384\text{ cm}^{-1}$  (related to  $\text{HCONH}_2$ , which are enhanced when compared to pure  $\text{CH}_3\text{NH}_2$  ice samples),  $1679$  and  $1142\text{ cm}^{-1}$  ( $\text{CH}_3\text{CHNH}$ ), and  $2830$ ,  $1729$  and  $1493\text{ cm}^{-1}$  ( $\text{H}_2\text{CO}$ ). Dehydrogenation of  $\text{CH}_2\text{NH}$  produces  $\text{HCN}$ .  $\text{HCN}$  was not identified in  $\text{CH}_3\text{NH}_2:\text{H}_2\text{O}$  ice mixture. As it was observed in pure  $\text{CH}_3\text{NH}_2$  ice samples,  $\text{HCN}$  tends to react, producing  $\text{CN}^-$ , and  $\text{OCN}^-$  species, which were identified by their absorptions at  $2080$  and  $2162\text{ cm}^{-1}$ , respectively.  $\text{CH}_3\text{NH}_2$  molecules can accept hydrogen atoms from  $\text{HCNO}$  and  $\text{HCN}$ , to produce the corresponding methylammonium salts ( $[\text{CH}_3\text{NH}_3^+ \text{CN}^-]$  and  $[\text{CH}_3\text{NH}_3^+ \text{OCN}^-]$ ). IR bands at  $2645$  and  $2552\text{ cm}^{-1}$  are indicative of the presence of  $\text{CH}_3\text{NH}_3^+$ .

As it could be expected, IR spectra shown in Fig. 8b and Fig. 8c show that the presence of  $\text{H}_2\text{O}$  diminishes  $\text{CH}_3\text{CN}$  and  $\text{CH}_3\text{CH}_2\text{NH}_2$  formation, while the formation of oxygenated compounds, such as  $\text{OCN}^-$  and  $\text{HCONH}_2$  is enhanced.

### 3.5 Irradiation of $\text{H}_2\text{O}:\text{CH}_3\text{OH}:\text{NH}_3$ ice analogs

We performed another experiment for comparison of the residue spectra obtained from methylamine-bearing ices with the better known residue made by irradiation and warm-up of the  $\text{H}_2\text{O}:\text{CH}_3\text{OH}:\text{NH}_3$  (20:1:1) ice mixture. This experiment was discussed in previous works (i. e. Bernstein et al. 1995; Muñoz Caro & Schutte 2003), and in this work, we only focus on the residue. This experiment served to check the formation of a "classical" residue under the UHV conditions of ISAC. The IR spectrum of this residue, presented in Fig. 16, is similar to the one reported in previous works.

### 3.6 Synthesis of large organics during warming up of UV irradiated $\text{CH}_3\text{NH}_2$ ice samples.

The reduced mobility of most species at the low temperatures present in interstellar ice mantles ( $10\text{--}20\text{ K}$ ), and reproduced in our experiments, inhibits the formation of large species prior to the warm-up phase. Furthermore, the relatively low column density values of methylamine ices from Exps. 2, 6 and 7 (see Table 1) prevented us from the detection of larger organic molecules. The irradiation of thicker methylamine ices gives us the possibility to detect larger species with our IR spectrometer. Fig. 12 shows IR spectra recorded after thermal desorption of methylamine molecules, from  $180\text{ K}$  to  $300\text{ K}$ . Bands located at  $3345$  and  $3321\text{ cm}^{-1}$  are related to the symmetric and antisymmetric modes of  $\text{NH}_2$  groups, that is, primary amines, at  $180\text{ K}$ . As the temperature increases, both vibration modes are merged, becoming indistinguishable above  $240\text{ K}$ . The same trend is observed for  $\text{CH}_3$  groups, as the band at  $2948\text{ cm}^{-1}$  disappears at the same temperature.  $\text{NH}_2$  and  $\text{CH}_3$  groups can be only bonded to one group, in other words, they are located at the end of the molecules or in branched species. The absence of these groups at larger temperatures is originated by two processes: thermal desorption of species to the gas phase, and the formation of larger chains and cyclic compounds that are refractory at those temperatures. Bands located in the  $1575\text{--}1625\text{ cm}^{-1}$  range, which remain at  $300\text{ K}$ , may be indicative of the presence of cyclic aromatic compounds.

Three different methylamine dimers can be formed from UV irradiation of methylamine,  $\text{CH}_3\text{--NH--CH}_2\text{--NH}_2$  (**Dimer A**),  $\text{CH}_3\text{--NH--NH--CH}_3$  (**Dimer B**), and  $\text{NH}_2\text{--CH}_2\text{--CH}_2\text{--NH}_2$  (**Dimer C**). The three dimers have the same molecular mass, hampering its unequivocal identification. Therefore, the most likely interpretation of the results is discussed in this work, although other species may contribute to the measured ion current of each of the  $\frac{m}{z}$  values. Fig. 13 suggests the presence of the three dimers in Exp. 8. From  $125\text{ K}$ , the ion current measured for  $\frac{m}{z} = 58$  and  $59$  could be related to the desorption of **Dimer B**. The presence of methyl groups at both ends decreases the capability of the central  $\text{NH}$  groups to form hydrogen bonds due to steric interactions, thus reducing their thermal desorption temperature. In fact, although the molecular mass of **Dimer B** doubles that of methylamine, the absence of hydrogen bonds in **Dimer B** determines the codesorption of both species. It is not surprising that hydrogen bonds highly modify the intermolecular interactions. As an example the high desorption temperature of pure  $\text{NH}_3$  ice,  $95\text{ K}$ , compared to pure  $\text{CH}_4$  ice,  $40\text{ K}$ , is due to H bonds in  $\text{NH}_3$  ice (e.g. Carrascosa et al. 2020; Martín-Doménech et al. 2018).

**Dimer C** is expected to be formed preferentially over the other dimers via reaction  $\text{NH}_2\text{CH}_2\cdot + \text{NH}_2\text{CH}_2\cdot$ , as methyl groups are more reactive at low temperatures than  $\text{NH}$  groups (see Sect. 3.4). The two  $\text{NH}_2$  groups at both ends enhances the formation of hydrogen bonds, thus retarding thermal desorption of **Dimer C** to  $211\text{ K}$ . Furthermore, the mass spectra of **Dimer B** and **Dimer C** are compared in Fig. 15 to the one measured for the  $211\text{ K}$  peak with our QMS. Its profile highly differs from **Dimer B**, in particular the low intensities of  $\frac{m}{z} = 45$  and  $60$ . On the contrary, the measured mass spectrum is more similar to **Dimer C**. It is not clear if the differences observed between the experimental data and the reported mass spectrum of **Dimer C** are due to variation in the fragmentation pattern due to the use of different instruments (i. e. NIST database versus our QMS), or whether there is contribution

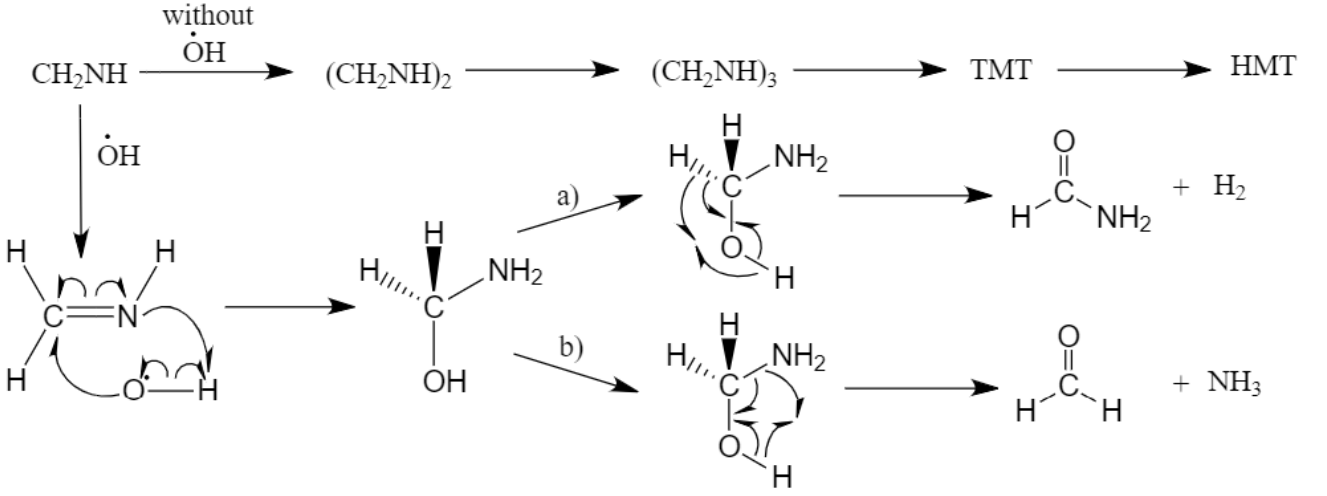


**Figure 11.** Chemical reactions of methylenimine molecules with and without surrounding OH radicals, formed from  $\text{H}_2\text{O}$  dissociation under UV photons. The presence/absence of water determines the preferential formation of formamide and formaldehyde, or HMT, respectively. Formamide,  $\text{HCONH}_2$ , and formaldehyde,  $\text{H}_2\text{CO}$ , can be formed at low temperature from radical reactions induced by UV photons (Bossa et al. 2009b).

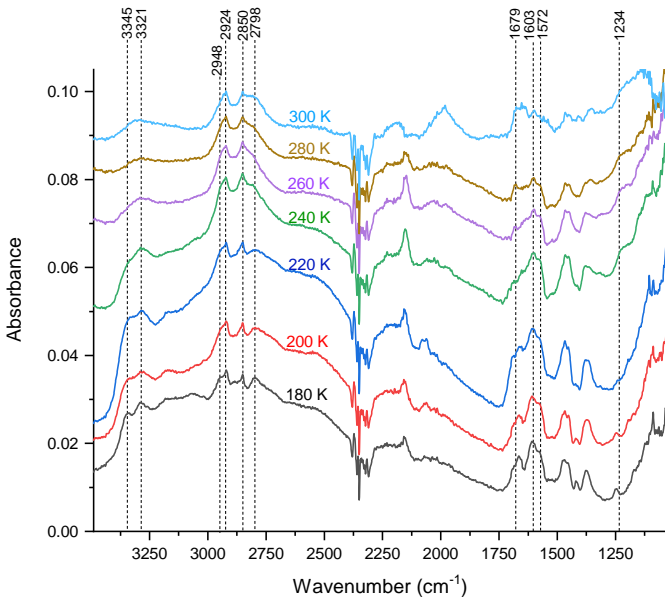


**Figure 12.** Evolution of the IR spectrum during warming up of a pure  $\text{CH}_3\text{NH}_2$  ice sample (Exp. 4).

of a codesorbing species in our experiment, such as **Dimer A**. Nevertheless, mass spectrum of **Dimer B** shows a preferential rupture of methyl groups, providing an intense ion current for  $\frac{m}{z} = 45$ .  $\frac{m}{z} = 45$  in the mass spectrum at 211 K in our experiments is marginal, suggesting that desorbing species do not contain methyl groups.

As it will be discussed later on, thermal desorption of TMT was observed at 290 K (see Fig. 13). TMT is likely formed from the reaction between three methylenimine units. Desorption of TMT molecules is therefore indicative of a previous formation of **Dimer A**, and its subsequent reaction to form the more stable 6-member cyclic TMT. Reactivity of the three dimers is then explained by the preferential reactivity of  $\text{CH}_x$  radicals when compared to  $\text{NH}_x$

radicals. Reactivity between two  $\text{CH}_2$  groups of  $\text{NH}_2\text{CH}_2\cdot$  radicals produces **Dimer C**. However, **Dimer C** cannot further react, as both ends contain  $\text{NH}_2$  groups. **Dimer B** formation is hampered, as it requires two  $\text{NH}$  groups to react and they react at temperatures higher than  $\text{CH}_x$  radicals. **Dimer A** is thus the only dimer able to form at relatively high ratios, and to further react to produce larger species.

TPD data in Fig. 13 suggests the formation of TMT molecules and its thermal desorption at 290 K. Signals recorded for  $\frac{m}{z}$  ratios larger than 87 did not show any increase at 290 K. Thus,  $\frac{m}{z} = 87$ , should be the molecular ion ( $\text{M}^+$ ), which coincides with the molecular mass of TMT. Despite the low ion current measured for  $\frac{m}{z}$  ratios in right panel of Fig. 13, the absence of any signal at 290 K for larger  $\frac{m}{z}$  ratios (e. g.  $\frac{m}{z} = 129$ , shown in Fig. 13), together with the blank experiment (Fig. 14), ensure the reliability of the measured ion current. The most intense fragment is obtained for  $\frac{m}{z} = 86$  ( $\text{M}^+ - 1$ ), followed by  $\frac{m}{z} = 85$  ( $\text{M}^+ - 2$ ). Vinogradoff et al. (2012) and references therein reported polymerization of  $\text{CH}_2\text{-NH}$  molecules to produce polymethylenimine (PMI,  $(-\text{CH}_2\text{NH-})_n$ ). No IR bands related to PMI, however, were detected in our experiments. Instead, the molecular ion,  $\frac{m}{z} = 87$ , suggests a cyclic species formed by three  $\text{CH}_2\text{-NH}$  units. A linear molecule formed from  $\text{CH}_2\text{NH}$  polymerization will imply very reactive  $\text{CH}_2$  and  $\text{NH}$  ends, and such molecules will further polymerize, or incorporate  $\text{CH}_3/\text{NH}_2$  ends, thus changing the mass of the molecular ion. Finally, the presence of  $\frac{m}{z} = 58$ , with no contribution of  $\frac{m}{z} = 59$  and 60, further suggest the presence of TMT. The loss of a  $-\text{CH}_2\text{-NH-}$  fragment of TMT will give rise to  $\frac{m}{z} = 58$ , but no  $\frac{m}{z} = 59$  or 60 fragments can be easily obtained from fragmentation of TMT molecules.

The presence of  $\text{CH}_2$  and  $\text{NH}$  groups at room temperature and the absence of  $\text{CH}_3$  (between  $3000 - 2948 \text{ cm}^{-1}$ ) and  $\text{NH}_2$  (only one band is observed between  $3450 - 3300 \text{ cm}^{-1}$ , while  $\text{NH}_2$  groups would provide the symmetric and antisymmetric N-H stretching modes) absorption features at this temperature, as shown in Fig. 12, suggests that **Dimer A** reacts to form larger species. The addition of an aminomethyl,  $\text{NH}_2\text{CH}_3$ , group produces TMT. The latter

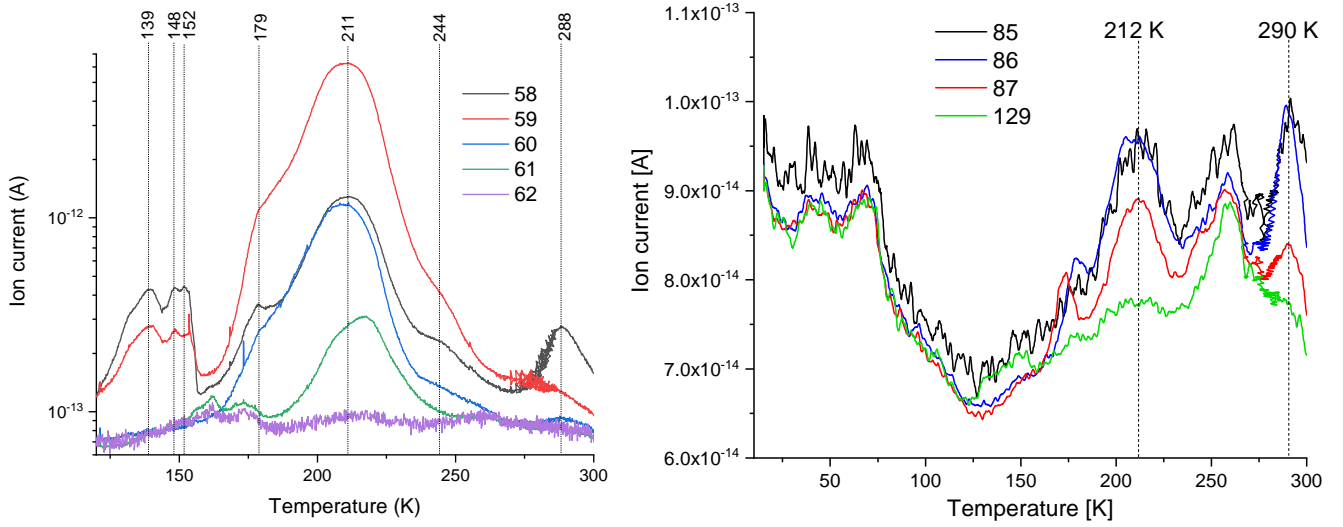


**Figure 13.** Warming up of an irradiated  $\text{CH}_3\text{NH}_2$  ice sample. Left: recorded QMS signal for  $\frac{m}{z} = 58, 59, 60, 61$  and  $62$ . These  $\frac{m}{z}$  fragments are representative of methylamine dimers. The molecular ion of non-covalent and covalent methylamine dimers has  $\frac{m}{z} = 62$  and  $60$ , respectively. Right: recorded QMS signal for molecular ion of TMT ( $\frac{m}{z} = 87$ ) as well as its corresponding M-1 and M-2 fragments (86 and 85, see text). No molecule is expected to desorb with a  $\frac{m}{z}$  ratio of 129, it was used for reference.

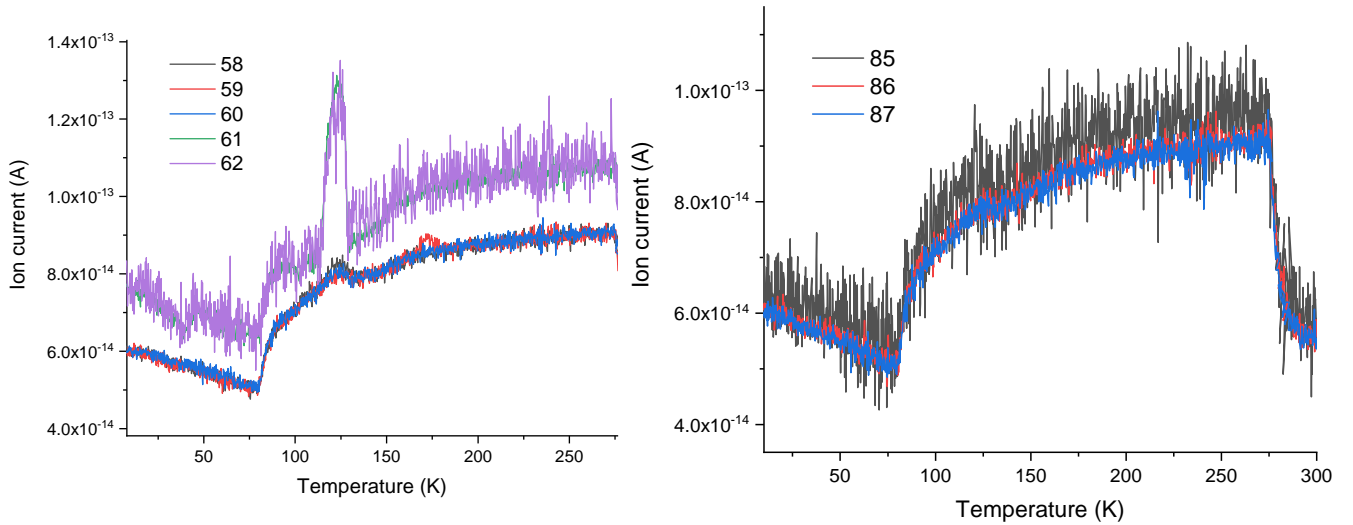


**Figure 14.** Warming up of a pure  $\text{CH}_3\text{NH}_2$  ice without any irradiation period. Left: recorded QMS signal for  $\frac{m}{z} = 58, 59, 60, 61$  and  $62$ , representing  $\frac{m}{z}$  ratios for methylamine dimers, being the non-covalent dimer ( $\frac{m}{z} = 62$ ) the most abundant species. Right: recorded QMS signal for  $\frac{m}{z} = 85, 86, 87$  in the same experiment, where no TMT formation is expected, in contrast to Fig. 13.

was observed to co-desorb with **Dimer C** at 212 K, but also at 290 K, by its molecular mass fragment,  $\frac{m}{z} = 87, 86$  and  $85$  (see Fig. 13).

To further confirm the formation of the dimers and larger species upon UV irradiation, the warming up of a non-irradiated methylamine ice is shown in Fig. 14. The ion current measured for  $\frac{m}{z} = 58 - 62$  is different to the one recorded for irradiated methylamine. Covalent dimers have a  $\frac{m}{z} = 60$ , therefore, their fragmentation give rise to  $\frac{m}{z}$  ratios below or equal to 60. From Fig. 14, it can be concluded that  $\frac{m}{z} = 61$  and  $62$  were present during the desorption with negligible contribution from  $\frac{m}{z} = 58, 59$ , and  $60$ . The most likely explanation is that the absence of radical species prevents the formation of covalent dimers, but hydrogen

bond interaction will hold pairs of molecules together, forming non-covalent  $(\text{CH}_3\text{NH}_2)_2$  dimers.

Possible formation of HMT in  $\text{CH}_3\text{NH}_2$  ice samples was also explored. Fig. 16 shows the IR spectrum of a  $\text{CH}_3\text{NH}_2$  ice sample at 300 K. Comparison with the experimental HMT spectrum suggests that HMT is formed in low  $\text{H}_2\text{O}$  containing  $\text{CH}_3\text{NH}_2$  ice samples. The organic residue remaining from the  $\text{H}_2\text{O}:\text{CH}_3\text{OH}:\text{NH}_3$  ice sample, shown in Fig. 16, displays more intense bands which can be related to HMT (816, 1005, 1234, 1458, and  $2868 \text{ cm}^{-1}$ ), reinforcing the formation of HMT through the mechanism show in Fig. 1. As shown in Fig. 17, 1004 and  $1234 \text{ cm}^{-1}$  IR features can be detected from 230 K, confirming that TMT can react to

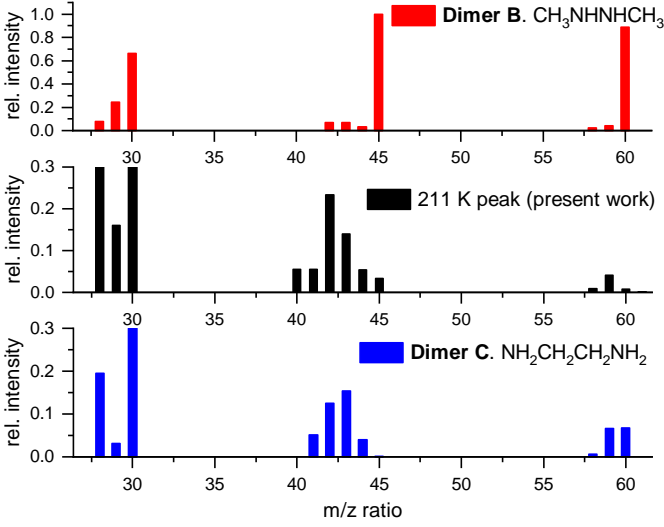


**Figure 15.** Mass spectra of **Dimer B** (top) and **Dimer C** (bottom) taken from NIST database. Relative intensities measured in our experiments during the desorption of the 211 K peak shown in Fig. 13 are shown for comparison (middle). To our knowledge, the mass spectrum of **Dimer A** has not been published. **Dimer A** might contribute to  $\frac{m}{z} = 28, 29, 40$  and  $42$ .  $\frac{m}{z} = 28$  and  $30$  have roughly the same intensity in the middle spectrum.

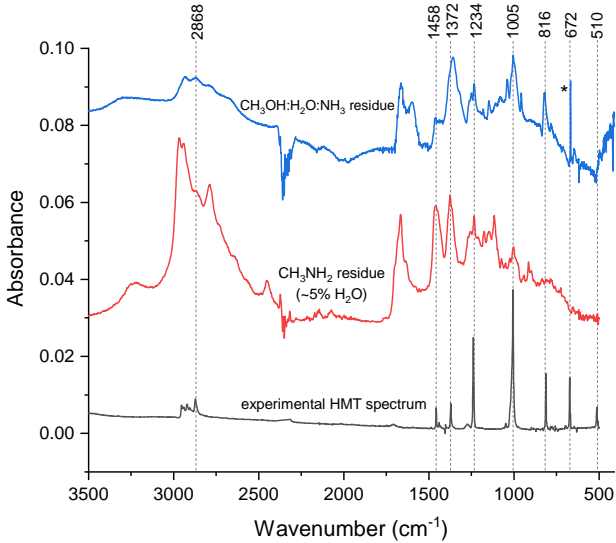


**Figure 16.** Bottom: Experimental IR spectrum of HMT shown for comparison. Middle: IR spectrum of an irradiated methylamine ice warmed up at 300 K (Exp. 8). Top: IR spectrum of an irradiated  $\text{H}_2\text{O}:\text{CH}_3\text{OH}:\text{NH}_3$  (20:1:1) ice sample warmed up at 300 K. The band labelled with an \* is due to impurities present in the substrate.

form HMT at this relatively low temperature, what may explain the absence of IR bands related to TMT, as compared to the theoretical spectrum in Fig. 2. Increasing temperatures, as explained above, cause the thermal desorption of remaining TMT molecules, while HMT remains in the refractory residue.

No HMT formation was observed in  $\text{CH}_3\text{NH}_2:\text{H}_2\text{O}$  ice samples. The presence of  $\text{H}_2\text{O}$  molecules drives the chemistry of methylamine towards the formation of oxygenated compounds. Water molecules inhibit polymerization of methylenimine,  $\text{CH}_2\text{NH}$ ,

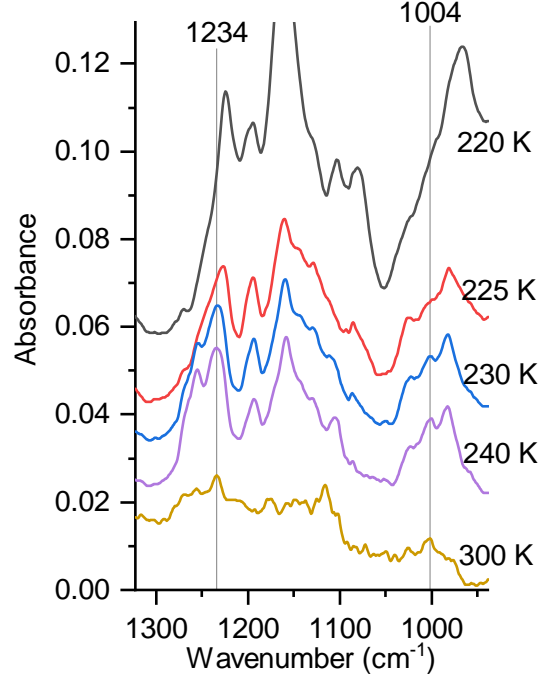


**Figure 17.** IR spectra during the warm-up of an irradiated  $\text{CH}_3\text{NH}_2$  ice. IR features related to HMT at  $1004$  and  $1234\text{ cm}^{-1}$  become clearly visible from 230 K.

see Fig. 11. Instead,  $\text{CH}_2\text{NH}$  is hydrolyzed to form formamide and formaldehyde.  $\text{CH}_3\text{OH}:\text{H}_2\text{O}:\text{NH}_3$  ice samples, however, showed an increased HMT formation upon addition of water.  $\text{H}_2\text{CO}$  is very efficiently formed from  $\text{CH}_3\text{OH}$  molecules, and  $\text{H}_2\text{O}$  is required to avoid formaldehyde polymerization. Thus, the presence of  $\text{H}_2\text{O}$  favours, in this case, condensation reaction between  $\text{H}_2\text{CO}$  and  $\text{NH}_3$  to produce  $\text{CH}_2\text{NH}$ , which cannot be obtained by other routes.

#### 4 CONCLUSIONS

The reactivity of  $\text{CH}_3\text{NH}_2$  ice under interstellar conditions was studied in the pure form, in an inert matrix (Xe), and mixed with  $\text{H}_2\text{O}$  in the ice, to mimic a more realistic astrophysical scenario. Methylamine-bearing ices were grown at low temperature (8 K) under UHV, and submitted to UV irradiation. From this work, several conclusions can be extracted:

- Methylamine thermal desorption is strongly dependent on its environment in the ice. The intermolecular forces established between methylamine and other species may cause thermal desorption to shift from 106 K to more than 150 K.
- The higher destruction rate of methylamine ice in an inert matrix suggests that a larger fraction of radicals can recombine in pure  $\text{CH}_3\text{NH}_2$  ice to reform the parent methylamine molecule. Xe isolated  $\text{CH}_3\text{NH}_2$ , however, does not trap hydrogen atoms, preventing reformation of  $\text{CH}_3\text{NH}_2$  molecules.

- $\text{H}_2$  molecules were not found to desorb when hydrogen bonds are established. Therefore,  $\text{CH}_3\text{NH}_2$  and  $\text{CH}_3\text{NH}_2:\text{H}_2\text{O}$  ice samples showed lower  $\text{H}_2$  subtraction compared to isolated  $\text{CH}_3\text{NH}_2$  molecules in the  $\text{CH}_3\text{NH}_2:\text{Xe}$  ice mixture. Irradiation of

pure CH<sub>4</sub> ice samples, which cannot form hydrogen bonds, showed an ion current for H<sub>2</sub> molecules 100 times higher than the one measured in irradiated CH<sub>3</sub>NH<sub>2</sub> pure ice.

- The retention of hydrogen within the ice samples leads to the formation of hydrogenated compounds in CH<sub>3</sub>NH<sub>2</sub> and CH<sub>3</sub>NH<sub>2</sub>:H<sub>2</sub>O ice samples over matrix isolated CH<sub>3</sub>NH<sub>2</sub>:Xe ice sample.

- As suggested by, e. g., [Martín-Doménech et al. \(2018\)](#) and [Carrascosa et al. \(2020\)](#), CH· radicals are more reactive at low temperatures than NH· radicals. As a result, CH<sub>3</sub>-bearing compounds are abundant in the irradiated ice samples. CH<sub>3</sub>CHNH, CH<sub>3</sub>CN, CH<sub>3</sub>CH<sub>2</sub>NH<sub>2</sub> were detected in irradiated CH<sub>3</sub>NH<sub>2</sub> ice samples.

- Oxygenated compounds usually exhibit larger IR band strengths, facilitating their detection. OCN<sup>-</sup>, H<sub>2</sub>CO and HCONH<sub>2</sub> were also detected in the IR spectra of the CH<sub>3</sub>NH<sub>2</sub>:H<sub>2</sub>O ice mixture.

- At increasingly higher temperatures, the higher mobility of radicals enhances the formation of larger species. The formation of the three possible methylamine dimers (CH<sub>3</sub>NHNHCH<sub>3</sub>, NH<sub>2</sub>CH<sub>2</sub>CH<sub>2</sub>NH<sub>2</sub> and CH<sub>3</sub>NHCH<sub>2</sub>NH<sub>2</sub>) was discussed. NH<sub>2</sub>CH<sub>2</sub>CH<sub>2</sub>NH<sub>2</sub> was found to be the most favoured one, followed by CH<sub>3</sub>NHCH<sub>2</sub>NH<sub>2</sub>. TPD experiments showed the formation of the three dimers, desorbing around 140 K, 210 K and 244 K.

- Furthermore, comparing irradiated and non-irradiated methylamine ices, it was found that covalent dimers are obtained from UV-irradiation, and non-covalent (CH<sub>3</sub>NH<sub>2</sub>)<sub>2</sub> dimers are present even without any irradiation period.

- TMT was detected by thermal codesorption with NH<sub>2</sub>CH<sub>2</sub>CH<sub>2</sub>NH<sub>2</sub> and pure thermal desorption at 290 K. The presence of TMT and the relatively low abundance of CH<sub>3</sub>NHCH<sub>2</sub>NH<sub>2</sub> suggests that TMT may be formed from the reaction between this dimer and an aminomethyl (-CH<sub>2</sub>NH<sub>2</sub>) species.

- The absence of IR features that could be related to TMT suggest the rapid reaction of TMT molecules. Indeed, the formation of HMT was detected in UV irradiated CH<sub>3</sub>NH<sub>2</sub>-bearing ices at 230 K, long before HMT formation in the 'classical' H<sub>2</sub>O:CH<sub>3</sub>OH:NH<sub>3</sub> ice mixture, where HMT synthesis takes place near room temperature ([Muñoz Caro & Schutte 2003](#); [Vinogradoff et al. 2012](#)).

- The addition of H<sub>2</sub>O molecules to CH<sub>3</sub>NH<sub>2</sub> inhibits HMT formation. Water molecules react with methylenimine, driving the chemistry towards oxygenated compounds, such as formamide and formaldehyde. On the contrary, CH<sub>3</sub>OH:H<sub>2</sub>O:NH<sub>3</sub> ice mixtures require the presence of water molecules to prevent formaldehyde polymerization, enhancing the formation of HMT. Therefore, depending on the ice composition, water molecules play a different role regarding HMT formation.

## 5 ASTROPHYSICAL IMPLICATIONS

The UV absorption cross section of CH<sub>3</sub>NH<sub>2</sub> ice within the 120-180 nm range was reported in this work (see Fig. 5), measuring a value of  $5.6 \pm 0.8 \times 10^{-18}$  molecule cm<sup>-2</sup> for pure CH<sub>3</sub>NH<sub>2</sub> ice. The UV absorption spectrum makes it possible to calculate the photon energy absorbed by methylamine ice which can be incorporated into computational models to improve the accuracy of the simulations.

CH<sub>3</sub>NH<sub>2</sub> is of particular interest in astrochemistry, as it contains a C-N bond, which is present in most biological molecules such as aminoacids, DNA, or heterocyclic compounds. The first detection of methylamine in the gas phase of the interstellar medium by [Kaifu et al. \(1974\)](#) opened the possibility to include methylamine in solid phase ice models. Experimental simulations including methylamine have shown its potential to give rise to COMs ([Holtom et al. 2005](#); [Bossa et al. 2009a](#); [Lee et al. 2009](#); [Vinogradoff et al. 2013](#)). [Vinogradoff et al. \(2012\)](#) and references therein studied the formation mechanism of HMT and complex mixtures containing methylamine. This work focuses on the reactivity of pure methylamine ice at low temperature exposed to UV irradiation, as a primary step to understand its chemistry toward the formation of N-heterocycles, in particular TMT and HMT. The addition of water molecules approaches to a more realistic astrophysical scenario of ice mantle photoprocessing followed by warm-up.

Several COMs were formed (see Table 3). Among them, formamide, HCONH<sub>2</sub>, is one of the most studied ones due to its prebiotic potential to form a full variety of species which are known to be present in our metabolism ([Saladino et al. 2012](#)). The addition of H<sub>2</sub>O to the ice sample enhances the formation of HCONH<sub>2</sub>, which was first detected in the ISM in Sgr B2 molecular cloud ([Rubin et al. 1971](#)), and later on in 67P/Churyumov-Gerasimenko comet during the Rosetta mission ([Goesmann et al. 2015](#); [Altwegg et al. 2017](#)). H<sub>2</sub>O molecules, as it can be derived from Fig. 7, lead to a large overall dissociation of methylamine molecules, producing a more complex chemistry.

[Vinogradoff et al. \(2012\)](#) reported the formation mechanism of HMT starting from a ternary H<sub>2</sub>CO:NH<sub>3</sub>:HCOOH ice mixture. They found evidence for the formation of the protonated form of TMT (TMT<sup>+</sup>) as an intermediate species during HMT synthesis. They stated that HCOOH is crucial to stabilize CH<sub>2</sub>NH allowing its presence at larger temperatures, where TMT can be thermally formed. The detection of TMT in pure CH<sub>3</sub>NH<sub>2</sub> experiments, and the absence of HMT formation suggest that a complex synthesis is required to form HMT, in agreement with previous works ([Vinogradoff et al. 2012](#), and references therein). Furthermore, this study deeps in the formation of TMT, which can lead to the synthesis of other N-heterocycles under astrophysically relevant scenarios, similar to those observed from H<sub>2</sub>O:CH<sub>3</sub>OH/CO:NH<sub>3</sub> ice mixtures (see, for example [Meierhenrich et al. 2005](#); [Oba et al. 2019](#)). Formaldehyde, H<sub>2</sub>CO, which is negligible in our experiments, but efficiently formed from methanol, is required for the formation of more complex heterocycles ([Muñoz Caro & Schutte 2003](#); [Vinogradoff et al. 2012](#)).

Even though methylamine is a minor component in the gas of the interstellar medium, after accretion on ice mantles or direct formation in the ice, thermal desorption of other species in hot

cores or warm protoplanetary disk regions can increase the relative abundance of methylamine in ice mantles. Indeed, prior to the thermal desorption of methylamine molecules, other species, such as CO, CH<sub>4</sub>, NH<sub>3</sub>, O<sub>2</sub>, N<sub>2</sub> and CO<sub>2</sub>, should have sublimated to the gas phase. Therefore, UV-irradiation and thermal processing of the ice mantles can increase the relative abundance of methylamine photoproducts, promoting chemical reactions between them which may lead to the formation of COMs following the synthetic pathways presented in this work.

## 6 ACKNOWLEDGEMENTS

We would like to devote this paper to the memory of our long-term colleague and dearest friend professor Rafael Escribano from Spanish CSIC, whose advise and stimulating discussions we enjoyed so much. The Spanish Ministry of Science, Innovation and Universities supported this research under grant number AYA2017-85322-R and MDM-2017-0737 Unidad de Excelencia "María de Maeztu"– Centro de Astrobiología (CSIC-INTA). (AEI/FEDER, UE). P. C. G. acknowledges support from PGC2018-096444-B-I00. H. C. was supported by PhD fellowship FPU-17/03172. M. L. S. acknowledges Ministerio de Economía y Competitividad of Spain for the project AGL2016-80475-R and Comunidad Autónoma de Madrid (Spain) and European funding from FEDER program (project S2018/BAA-4393, AVANSECAL-II-CM).

## 7 DATA AVAILABILITY

The data underlying this article will be shared on reasonable request to the corresponding authors.

## REFERENCES

- Altwegg K., et al., 2017, *MNRAS*, **469**, S130
- Belloche A., Müller H. S. P., Menten K. M., Schilke P., Comito C., 2013, *A&A*, **559**, A47
- Bera P. P., Sandford S. A., Lee T. J., Nuevo M., 2019, *ApJ*, **884**, 64
- Bernstein M. P., Sandford S. A., Allamandola L. J., Chang S., Scharberg M. A., 1995, *ApJ*, **454**, 327
- Bøgelund E. G., McGuire B. A., Hogerheijde M. R., van Dishoeck E. F., Ligterink N. F. W., 2019, *A&A*, **624**, A82
- Bossa J. B., Duvernay F., Theulé P., Borget F., D’Hendecourt L., Chiavassa T., 2009a, *A&A*, **506**, 601
- Bossa J. B., Theulé P., Duvernay F., Chiavassa T., 2009b, *ApJ*, **707**, 1524
- Bossa J.-B., Borget F., Duvernay F., Danger G., Theulé P., Chiavassa T., 2012, *Australian Journal of Chemistry*, **65**, 129
- Briggs R., Ertem G., Ferris J. P., Greenberg J. M., McCain P. J., Mendoza-Gomez C. X., Schutte W., 1992, *Origins of Life and Evolution of the Biosphere*, **22**, 287
- Carrascosa H., Cruz-Díaz G. A., Muñoz Caro G. M., Dartois E., Chen Y. J., 2020, *MNRAS*, **493**, 821
- Chaabouni H., Diana S., Nguyen T., Dulieu F., 2018, *A&A*, **612**, A47
- Cottin H., Szopa C., Moore M. H., 2001, *ApJ*, **561**, L139
- Cruz-Díaz G. A., Muñoz Caro G. M., Chen Y. J., Yih T. S., 2014, *A&A*, **562**, A119
- D’Hendecourt L. B., Allamandola L. J., Grim R. J. A., Greenberg J. M., 1986, *A&A*, **158**, 119
- Danger G., Bossa J. B., de Marcellus P., Borget F., Duvernay F., Theulé P., Chiavassa T., D’Hendecourt L., 2011a, *A&A*, **525**, A30
- Danger G., Borget F., Chomat M., Duvernay F., Theulé P., Guillemin J. C., Le Sergeant D’Hendecourt L., Chiavassa T., 2011b, *A&A*, **535**, A47
- Dickens J. E., Irvine W. M., DeVries C. H., Ohishi M., 1997, *ApJ*, **479**, 307
- Durig J., Zheng C., 2001, *Structural Chemistry - STRUCT CHEM*, **12**, 137
- Durig J. R., Bush S. F., Baglin F. G., 1968, *J. Chem. Phys.*, **49**, 2106
- Durig J. R., Zheng C., Gounev T. K., Herrebout W. A., van der Veken B. J., 2006, *Journal of Physical Chemistry A*, **110**, 5674
- Dyke J. M., Lee E. P. F., Zamanpour Niavaran M. H., 1989, *International Journal of Mass Spectrometry and Ion Processes*, **94**, 221
- Ferraro J. R., Sill G., Fink U., 1980, *Applied Spectroscopy*, **34**, 525
- Förstel M., Bergantini A., Maksyutenko P., Góbi S., Kaiser R. I., 2017, *ApJ*, **845**, 83
- Fourikis N., Takagi K., Morimoto M., 1974, *ApJ*, **191**, L139
- Fox S. W., Windsor C. R., 1970, *Science*, **170**, 984
- Frisch M. J., et al., 2016, Gaussian–16 Revision C.01
- Gardner E. P., McNesby J. R., 1980, *Journal of Photochemistry*, **13**, 353
- Gardner E. P., McNesby J. R., 1982, *The Journal of Physical Chemistry*, **86**, 2646
- Goesmann F., et al., 2015, *Science*, **349**, 2.689
- González Díaz C., Carrascosa de Lucas H., Aparicio S., Muñoz Caro G. M., Sie N.-E., Hsiao L.-C., Cazaux S., Chen Y.-J., 2019, *MNRAS*, **486**, 5519
- Hagen W., Tielens A. G. G. M., Greenberg J. M., 1981, *Chemical Physics*, **56**, 367
- Hashiguchi K., Hamada Y., Tsuboi M., Koga Y., Kondo S., 1984, *Journal of Molecular Spectroscopy*, **105**, 81
- Herbst E., 1985, *ApJ*, **292**, 484
- Herbst E., van Dishoeck E. F., 2009, *ARA&A*, **47**, 427
- Holtom P. D., Bennett C. J., Osamura Y., Mason N. J., Kaiser R. I., 2005, *ApJ*, **626**, 940
- Jacox M. E., Milligan D. E., 1975, *Journal of Molecular Spectroscopy*, **56**, 333
- Jiménez-Escobar A., Giuliano B. M., Muñoz Caro G. M., Cernicharo J., Marcelino N., 2014, *ApJ*, **788**, 19
- Kaifu N., Morimoto M., Nagane K., Akabane K., Iguchi T., Takagi K., 1974, *ApJ*, **191**, L135
- Kim Y. S., Kaiser R. I., 2011, *ApJ*, **729**, 68
- Layer R. W., 1963, *Chemical Reviews*, **63**, 489
- Lee C.-W., Kim J.-K., Moon E.-S., Minh Y. C., Kang H., 2009, *ApJ*, **697**, 428
- Martín-Doménech R., Cruz-Díaz G. A., Muñoz Caro G. M., 2018, *MNRAS*, **473**, 2575
- Martín-Doménech R., Öberg K. I., Rajappan M., 2020, *ApJ*, **894**, 98
- Materese C. K., Nuevo M., Sandford S. A., Bera P. P., Lee T. J., 2020, *Astrobiology*, **20**, 601
- Meierhenrich U., Caro G., Schutte W., Thiemann W., Barbier B., Brack A., 2005, *Chem. Eur. J.*, **11**, 4895
- Meissner F., Schwiedessen E., Othmer D. F., 1954, *Industrial & Engineering Chemistry*, **46**, 724
- Mencos A., Krim L., 2018, *MNRAS*, **476**, 5432
- Milligan D. E., Jacox M. E., 1967, *J. Chem. Phys.*, **47**, 278
- Moore M. H., Hudson R. L., 2003, *Icarus*, **161**, 486
- Muñoz Caro G. M., Schutte W. A., 2003, *A&A*, **412**, 121
- Muñoz Caro G. M., Meierhenrich U., Schutte W. A., Thiemann W. H. P., Greenberg J. M., 2004, *A&A*, **413**, 209
- Muñoz Caro G. M., Jiménez-Escobar A., Martín-Gago J. Á., Rogero C., Atienza C., Puertas S., Sobrado J. M., Torres-Redondo J., 2010, *A&A*, **522**, A108
- Oba Y., Takano Y., Naraoka H., Watanabe N., Kouchi A., 2019, *Nature Communications*, **10**, 4413
- Oba Y., Takano Y., Naraoka H., Furukawa Y., Glavin D., Dworkin J., Tachibana S., 2020, *Nature Communications*, **11**
- Ogura K., Migita C., Yamada T., 1989, *Journal of Photochemistry and Photobiology A: Chemistry*, **49**, 53
- Ohishi M., Suzuki T., Hirota T., Saito M., Kaifu N., 2019, *Publications of the Astronomical Society of Japan*, **71**
- Rubin R. H., Swenson G. W. J., Benson R. C., Tigelaar H. L., Flygare W. H., 1971, *ApJ*, **169**, L39

- Ruzi M., Anderson D., 2012, [The Journal of chemical physics](#), 137, 194313
- Saladino R., Botta G., Pino S., Costanzo G., Di Mauro E., 2012, [Chem. Soc. Rev.](#), 41, 5526
- Sandford S. A., Allamandola L. J., 1993, [ApJ](#), 417, 815
- Sandford S. A., Nuevo M., Bera P. P., Lee T. J., 2020, [Chemical Reviews](#), 120, 4616
- Schnepp O., Dressler K., 1960, [J. Chem. Phys.](#), 33, 49
- Schutte W. A., Allamandola L. J., Sandford S. A., 1993, [Icarus](#), 104, 118
- Sivaraman B., Raja Sekhar B. N., Nair B. G., Hatode V., Mason N. J., 2013, [Spectrochimica Acta Part A: Molecular Spectroscopy](#), 105, 238
- Stolkin I., Ha T. K., Günthard H. H., 1977, [Chemical Physics](#), 21, 327
- Theule P., Borget F., Mispelaer F., Danger G., Duvernay F., Guillemin J. C., Chiavassa T., 2011, [A&A](#), 534, A64
- Urso R. G., et al., 2020, [A&A](#), 644, A115
- Vazart F., Calderini D., Puzzarini C., Skouteris D., Barone V., 2016, [Journal of chemical theory and computation](#), 12
- Vinogradoff V., Rimola A., Duvernay F., Danger G., Theulé P., Chiavassa T., 2012, [Physical Chemistry Chemical Physics \(Incorporating Faraday Transactions\)](#), 14, 12309
- Vinogradoff V., Fray N., Duvernay F., Briani G., Danger G., Cottin H., Theulé P., Chiavassa T., 2013, [A&A](#), 551, A128
- Wexler A., 1967, [Applied Spectroscopy Reviews](#), 1, 29
- Zhang B., et al., 2017, [Journal of Physical Chemistry A](#), 121, 7176
- Zhu C., Frigge R., Turner A. M., Abplanalp M. J., Sun B.-J., Chen Y.-L., Chang A. H. H., Kaiser R. I., 2019, [Physical Chemistry Chemical Physics \(Incorporating Faraday Transactions\)](#), 21, 1952

This paper has been typeset from a  $\text{\LaTeX}$  file prepared by the author.